Quaternary International xxx (xxxx) xxx

Contents lists available at ScienceDirect

Quaternary International

journal homepage: www.elsevier.com/locate/quaint

Sedimentological evolution of the Quibas site: High-resolution glacial/interglacial dynamics in a terrestrial pre-Jaramillo to post-Jaramillo sequence from southern Iberian Peninsula

Casto Laborda-López [a,*], David M. Martín-Perea [b,a,c], Elia Del Castillo [d], M. Asunción Alías Linares [d], Claudia Iannicelli [a], Shubham Pal [e,f], Xabier Arroyo [g], Jordi Agustí [a,h,i], Pedro Piñero [a,i]

[a] IPHES-CERCA, Institut Català de Paleoecologia Humana I Evolució Social, Zona Educacional 4, Campus Sescelades URV (Edifici W3), 43007, Tarragona, Spain
[b] Departamento de Geodinámica, Estratigrafía y Paleontología, Facultad de Ciencias Geológicas, Universidad Complutense de Madrid, 28040, Madrid, Spain
[c] Institute of Evolution in Africa, Covarrubias 36, 28010, Madrid, Spain
[d] Departamento de Química Agrícola, Geología y Edafología, Facultad de Química, Universidad de Murcia, Campus Espinardo, 30100, Murcia, Spain
[e] Departament de Geologia, Universitat Autònoma de Barcelona, 08193, Bellaterra, Spain
[f] ICP-CERCA, Institut Català de Paleontologia Miquel Crusafont, Universitat Autònoma de Barcelona, Edifici ICTA-ICP, Carrer de Les Columnes S/n, Campus de La UAB, 08193, Cerdanyola Del Vallès, Barcelona, Spain
[g] Unidad de Técnicas Geológicas, CAI de Ciencias de La Tierra y Arqueometría, Universidad Complutense de Madrid, Calle José Antonio Novais, 12, Sótano, 28040, Madrid, Spain
[h] ICREA, Institució Catalana de Recerca I Estudis Avançats, Pg. Lluís Companys 23, 08010, Barcelona, Spain
[i] Àrea de Prehistòria, Universitat Rovira I Virgili (URV), Avinguda de Catalunya 35, 43002, Tarragona, Spain

ARTICLE INFO

Keywords:
Early pleistocene
Spain
Marine isotope stage
Paleoclimatology
Karstic site
Mineralogical analysis

ABSTRACT

The sedimentary infill of the Quibas karstic site (Early Pleistocene, southern Spain) represents the only continuous succession with remains of continental vertebrates in Europe from pre-Jaramillo to post-Jaramillo age. The Quibas site, with a significant paleontological record, is dated between 1.1 and 0.9 Ma and offers a unique opportunity to carry out a paleoclimatic reconstruction of the time period immediately after the arrival of the first humans to western Europe. For this reason, defining the dominant sedimentary processes in the different stratigraphic units and the associated paleoenvironment is essential. The Quibas site is made up of two karstic features with two stratigraphic sequences: Quibas-Cueva, containing six lithostratigraphic units, and Quibas-Sima, which contains seven lithostratigraphic units. The detailed description and analyses of the stratigraphic sections have allowed the characterization of various autochthonous and allochthonous facies of cave deposits. Paleoclimatic proxies, inferred from sedimentological analyses, reveal a record of several alternating humid and arid phases resulting from the Early Pleistocene glacial-interglacial cycles, allowing correlation to the marine oxygen isotope record. The lowermost units (pre-Jaramillo) were deposited during a long-lasting interglacial, correlated to MIS 33–31. It was followed by an increase in aridity in the intermediate units of Quibas-Sima and uppermost unit of Quibas-Cueva (Jaramillo), revealing the beginning of a glacial period at the start of the Jaramillo subchron (1 Ma), which can be correlated to MIS 30. The upper Jaramillo and post-Jaramillo units suggest these were deposited in alternating periods of aridity and humid conditions, although less humid than the pre-Jaramillo period, probably representing the MIS 29 interglacial, the MIS 28 glacial and the MIS 27 interglacial.

1. Introduction

Understanding the climate backdrop of the Early Pleistocene (2.58–0.78 Ma) is pivotal for unravelling the climatic and ecological shifts that affected the diversity of European land mammals, including hominins, and the patterns of their migrations and extinctions. In this timeframe, the climate underwent cyclical variations influenced by Earth's astronomical-obliquity forcings, leading to 'glacial' and 'interglacial' phases lasting approximately 41 ka each (Lisiecki and Raymo, 2005). These fluctuations in climate led to 42 consecutive cycles of

* Corresponding author.
E-mail address: claborda@ujaen.es (C. Laborda-López).

https://doi.org/10.1016/j.quaint.2024.02.015
Received 22 November 2023; Received in revised form 26 February 2024; Accepted 27 February 2024

associated vegetation, oscillating between open landscapes during glacial periods and dense forested landscapes during interglacial periods (Leroy et al., 2011). Along the Early Pleistocene, there was an overall trend towards slightly cooler conditions, resulting in progressively extended glacial periods (Lisiecki and Raymo, 2005). This is evident in the increasingly prolonged presence of open landscapes, generally observed during both glacial epochs and the transitional phases between glacial and interglacial periods (Leroy et al., 2011). The Mid-Pleistocene Transition was characterized by a fundamental change in the Earth's climatic cyclicity, with a strong intensification of glacial periods (Head and Gibbard, 2005). At the end of the Early Pleistocene, intense longer-lasting glacial cycles were established that contrasted with the short interglacial pulses, and the cycle duration changed from 41 to 100 ka (Head and Gibbard, 2005; Lisiecki and Raymo, 2005).

In this context, the information obtained through the study of the Quibas site, located in southeastern Spain (Abanilla, Region of Murcia;

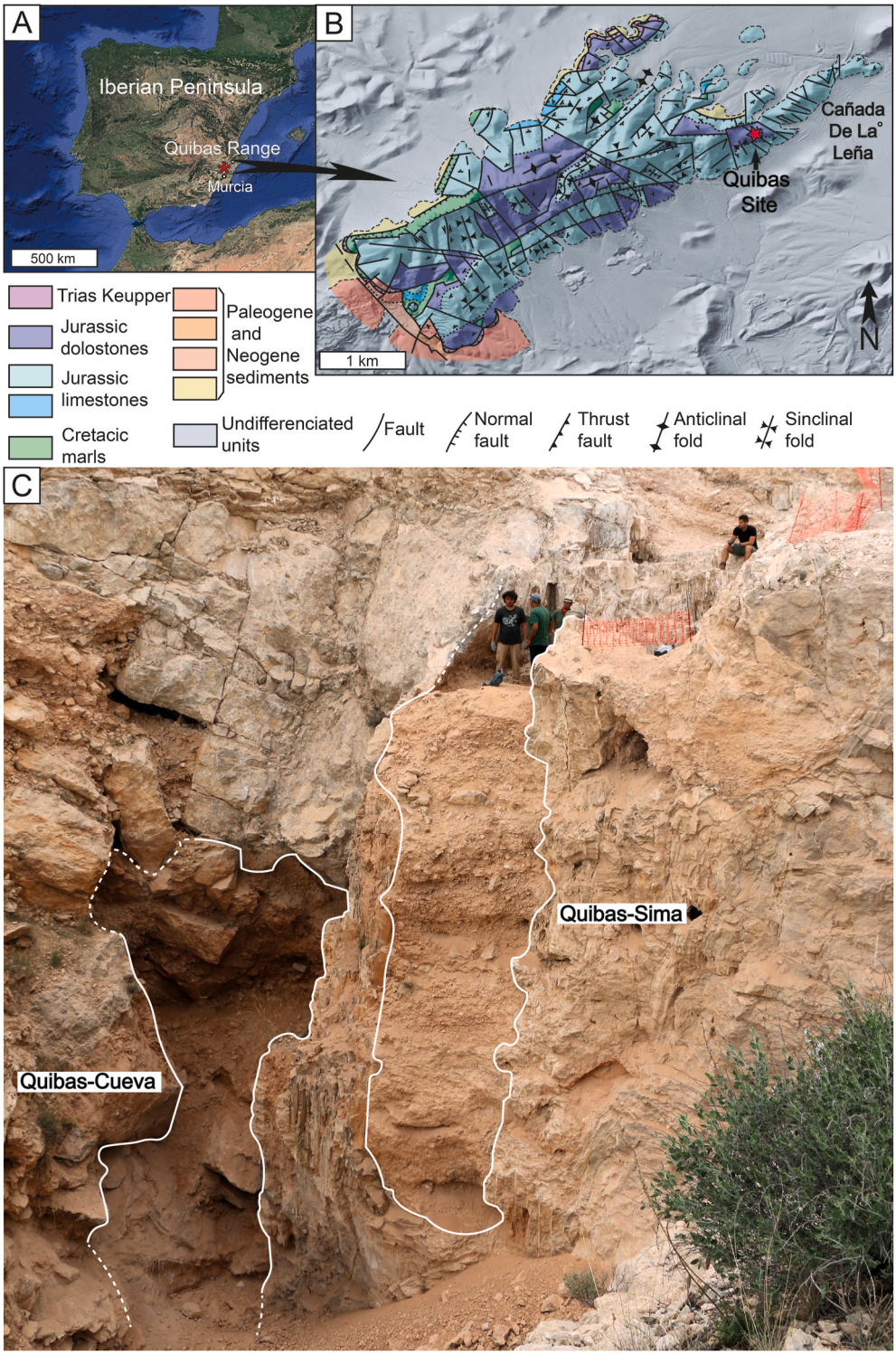

Fig. 1. Geographic and structural context of the Quibas site. A. Map of the Iberian Peninsula showing the location of Quibas. B. Geologic map of the Quibas Range with the location of the Quibas karstic complex. C. View of the two main structures of the Quibas site in 2015.

Fig. 1), represents a significant contribution to the understanding of the climatic events that took place at the end of the Early Pleistocene in south-western Europe (Piñero et al., 2020; Del Castillo et al., 2023). The site is located in an abandoned limestone quarry on the southeastern slope of the Quibas Range and comprised a karstic system (a cave) with different features (galleries and chasms) filled with sediments (Fig. 1). This karstic system infillings record impressive continental sequences dating from the late Early Pleistocene. With an age between 1.1 and 0.9 Ma, the Quibas site represents the only continuous sequence of terrestrial vertebrates of pre-Jaramillo to Jaramillo period in Europe (Piñero et al., 2020, 2022). Although levels of pre-Jaramillo and Jaramillo age have been detected in the Gran Dolina section (Atapuerca), these are levels with no record of continental vertebrates (Parés et al., 2018). Somewhat earlier than this time (at around 1.4–1.2 Ma), the first humans settled in the westernmost parts of the European continent (e.g. Carbonell et al., 2008; Toro-Moyano et al., 2013; Lozano-Fernández et al., 2019; Yravedra et al., 2021).

Karstic deposits provide an extraordinary record of cave formation, paleobiota, and the relationship between external and internal environmental conditions (Goldberg, 2000; Farrand, 2001; Pickering et al., 2007; Karkanas et al., 2008; Kourampas et al., 2009; Springer, 2012). Recognizing and characterizing different facies of these karstic infillings provides valuable information to elucidate the conditions under which they were formed, enabling the reconstruction of paleoenvironmental and paleoclimatic conditions (Farrand, 1975; Straus, 2001; Goldberg and Sherwood, 2006; Finlayson et al., 2008; Campaña et al., 2017).

So far, no evidence of human occupation has been found at the Quibas site, which could be related to a cooling that occurred between 1.15 and 1.12 Ma ago, immediately pre-dating the oldest levels of Quibas. The extreme conditions at the end of this cold phase would presumably have depopulated Europe during several successive glacial-interglacial cycles (Margari et al., 2023). However, since its discovery in 1994, this site has yielded fossil remains of more than 90 species, mainly vertebrates, including new taxa (Montoya et al., 1999, 2001; Carlos-Calero et al., 2006; Made et al., 2008; Alba et al., 2011; Blain et al., 2014; Sevilla et al., 2014; Pérez-García et al., 2015; Piñero and Alberdi, 2015; Piñero et al., 2015, 2016, 2020, 2022; Blain and Bailon, 2019; Rosas et al., 2022, 2023; Agustí et al., 2022). The Quibas karstic complex is formed by two main features, Quibas-Sima (QS) and Quibas-Cueva (QC), which are part of the same gallery. In Quibas-Sima, seven distinct detrital units have been distinguished (QS-1 to QS-7). According to magnetobiostratigraphic correlations, QS-1 has an age between 1.1 and 1.07 Ma, QS-2 to QS-5 between 1.07 and 0.99 Ma (Jaramillo subchron), and QS-6 and QS-7 between 0.99 and 0.9 Ma (Piñero et al., 2020, 2022). Quibas-Cueva comprises six different levels (QC-1 to QC-6). The most basal units of Quibas-Cueva are equivalent in age to QS-1 (1.1–1.07 Ma). Stratigraphic observations indicate that the highest level of Quibas-Cueva (QC-6) represents an extension of the QS-2/QS-3 level of Quibas-Sima.

The sedimentary record of the Quibas site can contribute significantly to expand our knowledge of the climatic changes that occurred during the transition from the Early to Middle Pleistocene. Specifically, a thorough examination of the different facies associations in the successive units of the Quibas stratigraphic sections is crucial for establishing a solid paleoenvironmental and paleoclimatic framework for the continental Early-Middle Pleistocene transition record in Southeast Iberia, close to the arrival of the first hominins.

This study aims to summarize, yielding new data, the results of the Quibas paleokarstic-complex site (Fig. 1), in which stratigraphic sections were studied to identify the different facies associations, the depositional environment and to interpret paleoenvironmental and paleoclimatic conditions. The high-precision chronology of the Quibas site offers the opportunity to correlate the detected continental paleoenvironmental shifts to the marine oxygen isotope record (Marine Isotopic Stages).

2. Geological and geomorphological setting

The Quibas Range is a part of the northeastern Betic Cordillera, and it is an open anticlinal fold ridge with a klippe structure of Middle Subbetic overlying Southern Prebetic materials. The calcareous massif of the Sierra de Quibas is 6 km in length and 2.5 km wide, and mainly consists of Mesozoic rocks, Lower Jurassic limestones, and dolostones (Fig. 1B; Azema and Montenat, 1975; Azema, 1977; Rodríguez Estrella et al., 2004). This massif underwent a neotectonic activity from the upper Miocene, manifesting in the presence of N–S and NE-SW sets of faults. From a geomorphological point of view, the Quibas Range presents karstic systems with different features; most of them were formed along these previous faults and diaclase sets (Rodríguez Estrella et al., 2004).

The site of Quibas is located in the eastern part of the Quibas Range. Specifically, it was found in an abandoned quarry that cut a part of the karstic system in which it is found the Quibas site (Montoya et al., 1999). The outcropping karstic system consists of different passages, including a ~5-m-wide, ~8-m-high gallery, and an unknown length (Quibas-Cueva), within which a chasm was developed in the zenithal part of the cave (Quibas-Sima) (see Fig. 1C). There are also secondary cavities infilled with laminar speleothems (flowstones). The strike of the main gallery and the secondary cavities is N30°E (Rodríguez Estrella et al., 2004). On the southwestern wall of the quarry, several collapses fill one of the original entrances of the cave. The entire dimensions of the cave are unknown due to the impossibility of exploring it as all the structures are filled with quaternary deposits that comprise the Quibas site.

The formation of the karstic Quibas system should have started in a phreatic regimen during the Pliocene (Rodríguez Estrella et al., 2004), when the endo-karstic system was formed like analogous caves in the southeast of the Iberian Peninsula (eg Walker et al., 2013). The karstic Quibas system shifted into a vadose regime during the Early Pleistocene, and the opening of different entrances enabled the deposition of the allochthonous sediments that fill the cavities (Montoya et al., 1999).

3. Materials and methods

3.1. Lithostratigraphic unit definition and sampling

Two different profiles were exposed and freshly scraped on the old quarry walls in the Quibas site. Additionally, new profiles have been exposed on excavation walls and surrounding areas that connect the two previous profiles, providing additional information. Lithostratigraphic units were described, measured and photographed. The descriptions of lithostratigraphic units were based on sediment texture, structure, color (hue, value, and chroma), and stratigraphic contacts.

Representative samples of each lithostratigraphic unit were collected from the freshly scraped exposures to carry out granulometrical and mineralogical analyses. Sieves sized 63–2000 μm were used for measuring grain size distribution. Following Blott and Pye (2012), sediment types have been classified based on particle size distributions.

3.2. Sedimentological and mineralogical analyses

15 g of unaltered samples from each lithostratigraphic level were homogenized by quartering and manually ground using an agate mortar, then sieved through a 50 μm metallic mesh. Bulk mineralogy powder X-ray diffraction (XRD) spectra were produced using a Philipps Analytical PW 1752 Cu Kα radiation X-ray diffractometer (graphite monochromator radiation Kα1 = 1540.6 nm), continuously recording diffraction spectra at 2θ angles from 2° to 68° with 0.02 stepping intervals and 1 s per step. Following Chung (1975), a semi-quantitative analysis was carried out using EVA software (Bruker), determining the Reference Intensity Ratios (RIR) of the existing phases and allowing the normalization of intensity calculations.

For a complete understanding of the clay mineral assemblage, one sample (QS-1.1) was prepared for oriented aggregates XRD method (OA)

by taking a further fraction (0.1–0.5 g) of the original sample and dispersing it with distilled water. The <0.5 μm fraction was separated and extracted according to Stoke's law and pipetted into a glass slide, where it was left to dry. The semi-quantitative analysis was carried out by using EVA software (Bruker) according to Srodon (1984) and Moore and Reynolds (1989), based on the reflective power applied over the measured areas of each mineral's main reflection peak (assuming that the sum of all clay minerals in the sample sums up to 100%).

Lastly, small chips were broken from representative rock blocks from lithostratigraphic units to expose fresh fracture surfaces representative of the micro-fabric and micro-texture of the rock, gold-coated and studied under a Scanning Electron Microscope (SEM). The SEM is equipped with an energy dispersive spectrometer (EDS) system for determining the chemical composition of small particles during SEM observations.

The samples were also subjected to electrical conductivity, ion chromatography, and inductively coupled plasma optical emission spectrometry (ICP-OES) using argon plasma. The electrical conductivity analysis allowed to identify the degree of salinity contained in the studied levels, with samples exceeding the value of 4 dSm^{-1} considered to present a notable salt content. The ion chromatography technique allowed us to quantify the content of anions (chloride, nitrate and sulphate) for samples with a conductivity greater than or equal to 4 dSm^{-1}, whereas the ICP-OES technique showed the content of cations present at these same samples.

3.3. Facies description

The sedimentological analysis is based on the facies association concept, which consists of assemblages of spatially and genetically related facies that are the expression of different sedimentary environments (White, 2007a). The terms "autochthonous" and "allochthonous" are used following Iacovello and Martini (2012) and Bosch and White (2018). The term autochthonous is used to indicate sediments derived within the cave (e.g. rock fall deposits). The term allochthonous is used for sediments transported into the cave (e.g. channel deposits). Chemical deposits (e.g. flowstones) are assumed to be autochthonous.

3.4. Paleonvironmental and paleoclimatic inferences

Cave fillings have been frequently used as paleoenvironment and paleoclimate indicators (Bull, 1981 Lawson, 1995; Woodward and Goldberg, 2001; Auler et al., 2009). Clastic and chemical cave sediments can provide essential data for local, regional and sub-continental reconstructions of climate change throughout the Quaternary period. Although caves provide a greater degree of protection for sediment from external erosion, they can present other problems such as disconformities, paraconformities, sediment and fossil reworking, or even inverted stratigraphies (Osborne, 1984), which is why they have not been as extensively used as other continental sedimentary deposits (Pons et al., 1989).

Paleoclimatic inferences from the Quibas sedimentary record have been based on the following assumptions: (1) Clay minerals can be used as a proxy to reconstruct paleoclimatic changes (Singer, 1980, 1984; Chamley et al., 1983, 1989; Thiry, 2000; Hong, 2010; Huang et al., 2020). The formation and transformation of clay particles primarily occurs during continental weathering and soil formation, with changes in temperature and precipitation playing a crucial role in controlling these processes (Kennett and Warkne, 1992); (2) The abundance and presence of certain minerals such as palygorskite, halite and gypsum can be indicative of arid and evaporative conditions outside the karstic system (Singer, 1979, 1989; Jones and Ng, 1988; Inglés and Anadón, 1991; Gurel, 2008; Kadir and Eren, 2008; Kadir et al., 2010; Ye et al., 2018); (3) Debris flows have been postulated to indicate dryness events where vegetation is less, allowing soil dragging (Brook and Nickmann, 1996; Brook et al., 1997; Auler et al., 2009). On the other hand, gravity flows are generally produced by a massive contribution of water that destabilizes the slopes, leading other authors to postulate that they indicate more humid moments (Pawelec, 2006; Kłapyta et al., 2016). They have been described in caves located in highly humid places such as New Guinea and Borneo (Gillieson, 1986; Dykes, 2007); and (4) Erosional processes within the cave are related to humid periods (Brook and Nickmann, 1996; Brook et al., 1997) or transitional periods between dry and humid events (Auler et al., 2009). Paleoclimatic interpretations from the sedimentary record and sedimentary facies changes should be taken cautiously since many variables are involved in a sedimentary environment. Therefore, these interpretations should be supported by other available paleoenvironmental indicators, such as microfauna analyses.

Paleoenvironmental interpretations based on clastic deposits should be approached with caution. Sedimentary deposits are influenced by various factors, not just the environment, although it is one of the most significant factors. To conduct paleoenvironmental interpretations at the Quibas paleontological site, we must assume that the sediment source originated from soil development on the slopes of the Sierra de Quibas, and that these soils were sensitive to local and regional climate changes. The paleoenvironmental interpretation of the facies at the Quibas paleontological site has been combined with new geomorphological, faunal, and pollen data.

4. Results

4.1. Quibas stratigraphic sequence

Quibas-Cueva (Fig. 2) and Quibas-Sima (Fig. 3) have been divided into six and seven lithostratigraphic units, respectively. Quibas-Cueva is a gallery 8 m high, 5 m wide and a yet unknown depth, although geophysical prospections reveal a minimum of 30 m. Quibas-Sima is 9 m deep and 2 m wide. As will be noted in the next section, both cavities are internally connected, lithostratigraphic unit QC-6 being a continuity of QS-2/3.

4.1.1. Quibas-Cueva section

The lowermost lithostratigraphic unit of Quibas-Cueva, QC-1, is further divided into two subunits, QC-1.1 and QC-1.2.

QC-1.1 subunit is the lowest level of the Quibas-Cueva section. It is a ~1-m-thick breccia composed of angular limestone and speleothem clasts (Fig. 2). The speleothem clasts are mainly fragments of flowstones from the walls and zenital speleothems. The matrix of this breccia is a pink (7.5 YR 7/4), poorly sorted, slightly gravelly muddy sand (Fig. 4; Table 1). These materials lay over a chaotic block accumulation cemented by a calcite speleothem that forms the cave floor. An accumulation of macrovertebrate fossils is attached to this cave floor, embedded in a cemented bone and bone fragment breccia.

QC-1.2 subunit is a ~0.5 to 1-m-thick clast-supported and poorly selected breccia with angular clasts with a scarce, reddish yellow (7.5 YR 7/6) (Fig. 2) polymodal gravelly mud matrix (Fig. 4; Table 1).

QC-2 unit consists of homogeneous gravelly sediment with sub-rounded clasts and a scarce, reddish yellow (7.5 YR 7/6) mud matrix (Figs. 2 and 4; Table 1), 0.2–0.7 m thick. The unit presents root bioturbation and contains polyhedral aggregates. The contact with the underlying unit is sharp, concave and irregular.

The QC-3 unit consists of a poorly sorted breccia with angular limestone clasts and boulders, speleothems and gelifraction plates (Fig. 2) with a slightly gravelly muddy sand matrix (Fig. 4; Table 1). This unit is ~0.3–0.5 m thick and displays a chaotic structure, with a sharp contact with the underlying materials.

QC-4 consists of a ~0.3–0.5-m-thick, reddish yellow (7.5 YR 6/6), poorly sorted gravelly mud with sub-rounded clasts and polyhedral aggregates (Fig. 2; Table 1). This unit comprises more than 40% mud (Fig. 4; Table 1). The contact with the previous unit is sharp and irregular. This unit has abundant microvertebrate remains, and areas with

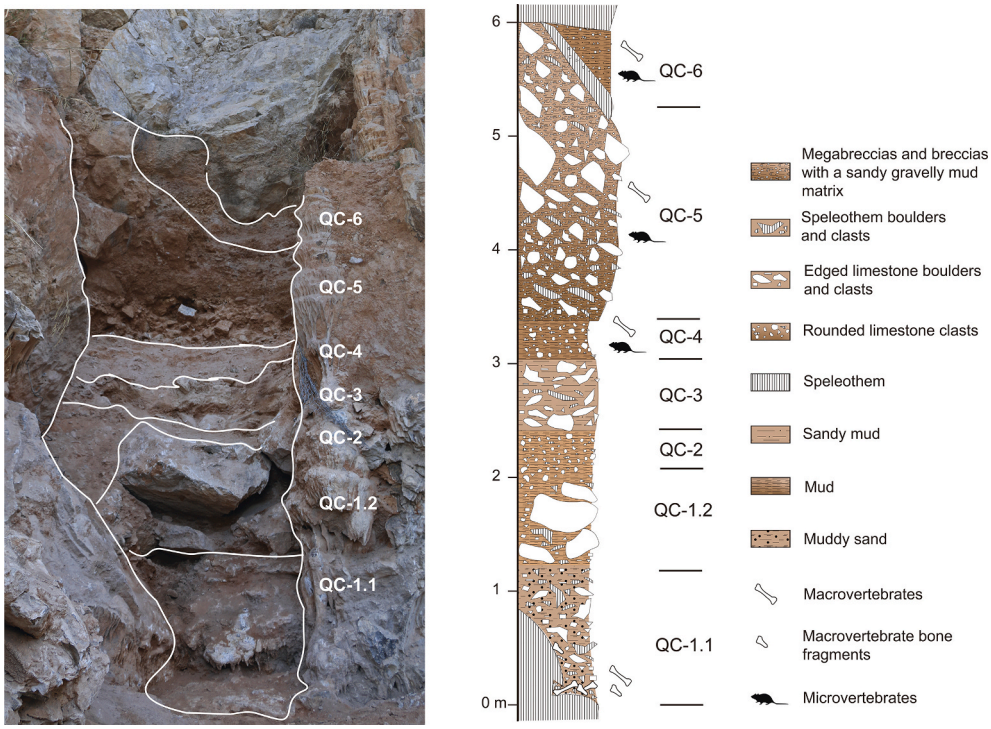

Fig. 2. Detailed stratigraphic section of Quibas-Cueva.

accumulation of large bones are common.

QC-5 is a 3-m-thick accumulation of large and very large boulders, some imbricated (Fig. 2). The matrix between the boulders and clasts is a polymodal muddy sand (Fig. 4, Table 1). The color of the matrix varies from strong brown (7.5 YR 5/6) at the bottom to pink (7.5 YR 7/4) towards the top. The top of the unit is sealed by a speleothem that is easily correlated with the speleothem on the top of the QS-1.3 unit in the Quibas-Sima section. Large mammal and microvertebrate bone remains are common.

QC-6 is the last lithostratigraphic unit and is in contact with the cave roof. This unit consists of a reddish yellow (7.5 YR 6/6) gravelly mud-rich sediment with a mix of subrounded and angular clasts (Figs. 2 and 4; Table 1). This unit connects laterally with the QS-2/QS-3 unit from the Quibas-Sima section. Towards the Quibas-Sima section, clasts become coarser and more angular, and the sand component increases in the matrix. There are both small and large vertebrate remains.

4.1.2. *Quibas-Sima section*

The Quibas-Sima section comprises seven differentiated lithostratigraphic units (QS-1 to QS-7) and two speleothems (S1 and S2; Fig. 3).

The lowermost lithostratigraphic unit, QS-1, is divided into three subunits: QS-1.1, QS-1.2 and QS-1.3. QS-1.1 consists of a 1.8-m-thick, massive, light red-brown (10 YR 7/3, 7.5 YR 8/4), polymodal sandy mud (76–79% of mud; Fig. 4), with fine gravel clasts, granules and small speleothem clasts. Towards the base of the unit, in contact with the basal speleothem, there is a 4-cm-thick level of poorly sorted muddy sandy gravel composed of speleothems and angular limestone clasts. Small vertebrate remains are abundant, especially in some organic-matter-rich bed sets.

QS-1.2 is a 0.3-m-thick, light-reddish (10 YR 7/4), cemented polymodal gravelly mud sediment (~46% of mud content; Fig. 4). It has yielded large mammal and microvertebrate bone fragments.

QS-1.3 consists of a 1.2-m-thick microstratified, light-brown (10 YR 8/4), moderately cemented and poorly sorted sandy mud (43% sand and 55% mud; Fig. 4). There are abundant bioturbations, scours and dissecation structures. It is rich in microvertebrate remains and also contains some large mammal bones.

Two speleothem layers overlie the uppermost part of the QS-1.3 subunit. The lower one (S1) has a laminar structure, whereas the upper one (S2) is thicker and consists of different successive types of speleothems in the same bedset: laminar, coralloid and massive speleothems (Caddeo et al., 2015).

During excavation campaigns, the contact between units originally described as QS-2 and QS-3 (Piñero et al., 2020) was not clearly identified, since the sedimentological differences between one and another were not significant. For this reason, in the present work, we consider QS-2 and QS-3 to be part of the same unit (hereafter referred to as QS-2/3).

Unit QS-2/3 is 2.7 m thick. The sediment of the first few centimeters above the underlying speleothem is similar to that of QS-1.3. The successive bedsets consist of microbreccia gravels and breccias with normal and inverse grading with a polymodal brown (7.5 YR 8/4) to reddish light-yellow (7.5 YR 8/4) muddy sand matrix that hosts some large boulders (Fig. 3). In the upper bedsets, there are some clast-supported coarse-grained breccias with large clasts with scarce or no matrix. This unit is rich in large and small vertebrate fossils.

QS-4 is a 1-m-thick breccia deposit composed of unimodal gravel and cemented muddy sand of reddish yellow color (7.5 YR 8/2). The lower scorured surface boundary is filled with boulders. The breccia is microstratified with discontinuous thin layers showing normal and inverse gradation. The upper bedset is composed of thin, cemented beds. The upper contact is sealed with a caliche (calcrete or dolocrete) and a scoured surface with a boulder deposit of Jurassic carbonates and speleothem fragments (Fig. 3). This unit has yielded both small and large vertebrate fossils.

QS-5 unit consists of a 1-m-thick well-microstratified breccia. This deposit contains three horizontal and parallel bedsets and two lenticular bedsets close to the upper contact. The lower horizontal bedsets are made of unimodal fine gravels (4–6 cm), either clast-supported with a planar fabric or matrix-supported in a pale brown (7.5 YR 7/6, 5 YR 6/6) muddy sand matrix (Fig. 3). The upper lenticular gravel beds are clast-supported and show normal and inverse gradation. This unit yielded no fossils other than gastropods.

QS-6 unit is a 1-m-thick breccia. The breccia is microstratified in four

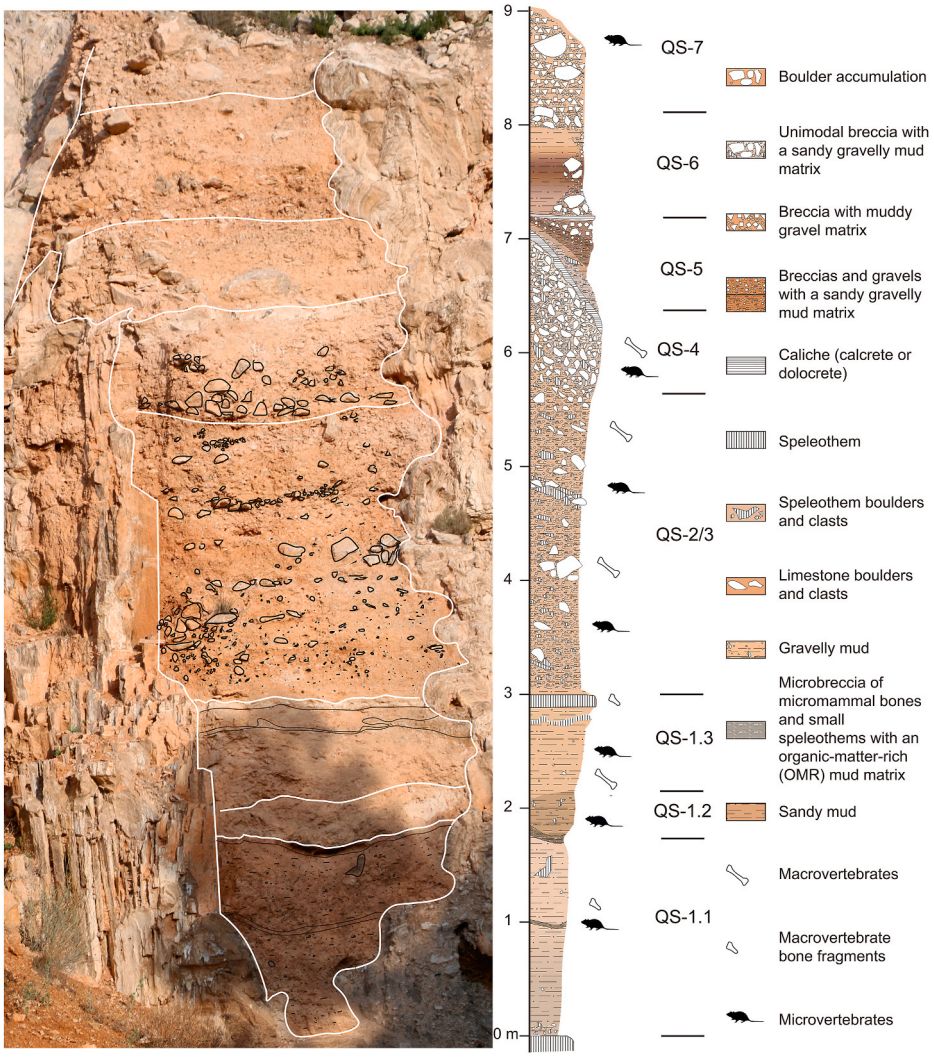

Fig. 3. Detailed stratigraphic section of Quibas-Sima.

bedsets of discontinuous and horizontal strata. These deposits are matrix-supported, in a pale brown (2.5 YR 6/4) muddy sand matrix with normal-inverse gradation (weakly developed), and contain abundant boulders (roughly 25 cm maximum elongated axis). The unit contains gastropod fossils, but vertebrates are absent. Laterally, this unit consists of a thick paleosol.

QS-7 is a 2.5-m-thick, poorly stratified, heavily cemented bimodal breccia. It is composed of medium and fine gravel with limestone and speleothem clasts. This unit has a clast-supported structure infilled with calcareous pale brown muddy sand. There are two beds composed of large boulders (speleothem fragments; Fig. 3). This unit has yielded scarce small vertebrate remains and has been entirely excavated.

4.2. Mineralogical analyses

4.2.1. Quibas-Cueva section

The scarce, slightly gravelly muddy sand matrix of unit QC-1.1 is mainly composed of calcite (34%), quartz (22%), clay minerals (21%), and dolomite-ankerite (11%), alongside smaller quantities of plagioclase, alkali feldspars, aragonite, hematite, and apatite (Table 2). Similarly, calcite (37%), quartz (21%), clay minerals (18%), and dolomite-ankerite (17%) are the most abundant minerals in unit QC-1.2 (Table 3). SEM observations reveal a clastic texture, where abundant sub-angular and sub-rounded calcite clasts with high sphericity are found alongside bigger, less spherical and more angular calcite, quartz, and feldspar clasts (Fig. 5A). Euhedral rhombic dolomite-ankerite crystals can be observed growing on pore walls, with palygorskite fibers as bridges on and between clasts and crystals (Fig. 5B).

Carbonate minerals such as dolomite-ankerite (31%) and calcite (28%) dominate the QC-2 mineral assemblage, followed by quartz (19%) and clay minerals (14%), and small quantities (<3%) of plagioclase, alkali feldspars, goethite, hematite, halite, and apatite (Table 2). The texture of QC-2 is clastic, composed of calcite, dolomite-ankerite, and quartz sub-rounded and rounded spherical clasts with clay aggregates.

Calcite (33%), quartz (25%), dolomite-ankerite (18%), and clay minerals (14%) are the most abundant mineral phases in the slightly gravelly muddy sand matrix of unit QC-3, alongside small quantities of plagioclase, K feldspars, aragonite, hematite, and apatite (Table 2). When observed under the SEM, the QC-3 unit is very porous, with abundant micrite (calcitic and dolomitic composition), euhedral rhombic dolomite-ankerite crystals formed on top of other minerals and on pore walls, and fibrous palygorskite masses growing as bridges on and between all other clasts (Fig. 6D).

The muddy deposits of unit QC-4 are mainly composed of quartz (30%), clay minerals (30%), and calcite (18%), with minor amounts of dolomite-ankerite, plagioclase, alkali feldspars, aragonite, goethite, hematite, and apatite (Table 2). SEM observations show that the QC-4 unit is detritic, with allochthonous quartz, feldspar, and calcite angular and sub-angular low-sphericity clasts with abundant smectite

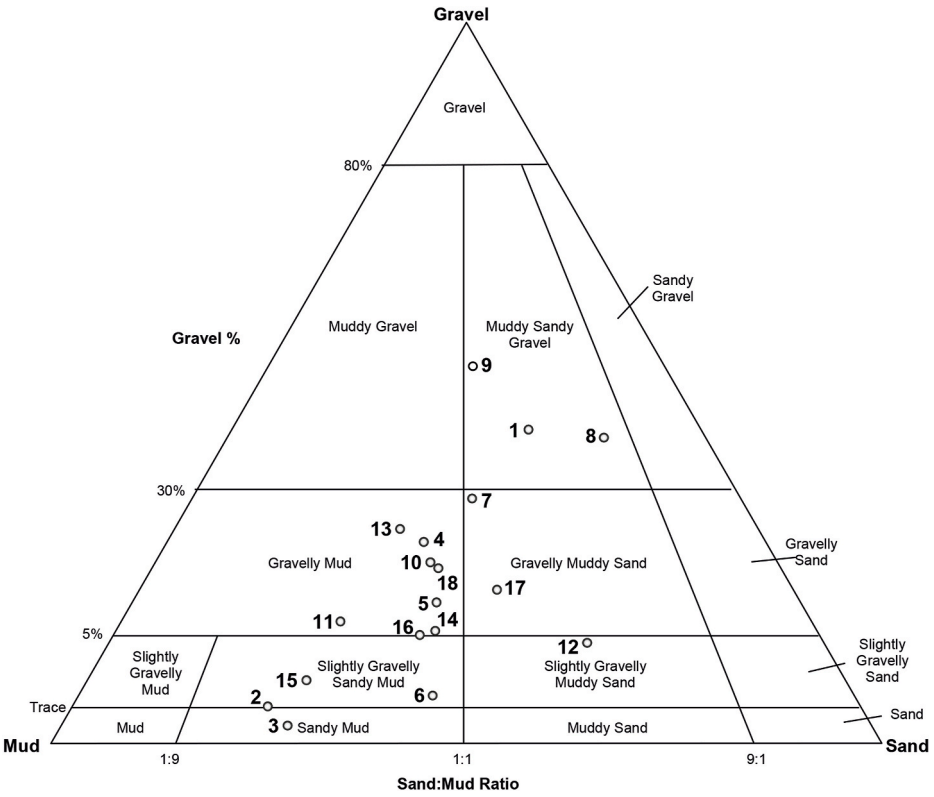

Fig. 4. Granulometries of the Quibas-Cueva and Quibas-Sima lithostratigraphic units projected on a ternary diagram (gravel-sand-mud trigon) according to Blott and Pye (2012). 1, QS-1.1 Base. 2, QS-1.1 OMR. 3, QS-1.1 Top. 4, QS-1.2 OMR. 5, QS-1.2.6, QS-1.3.7, QS-2/3.8, QS-2/3 Top. 9, QS-4.10, QS-5.11, QS-6.12, QC-1.1.13, QC-1.2.14, QC-2.15, QC-3.16, QC-4.17, QC-5 Base. 18, QC-6 Base.

Table 1
Particle size analyses.

Sample	>2000	1000	500	250	125	65	65>	Gravel	Sand	Mud
QS-1.1 Base	41.1	3.5	5.3	7.9	9.3	11.5	21.4	41	38	21
QS-1.1 OMR	1.0	2.0	3.9	2.9	5.9	4.4	79.9	1	19	80
QS-1.1 Top	0.3	0.3	4.7	6.7	5.1	6.1	76.7	0	23	77
QS-1.2 OMR	22.7	3.2	3.8	3.8	12.0	8.2	46.4	23	31	46
QS-1.2	12.1	1.7	7.6	9.0	12.1	7.6	49.8	12	38	50
QS-1.3	1.7	1.3	8.8	11.7	12.5	8.8	55.4	2	43	55
QS-2/3	39.8	12.3	13.2	8.4	8.4	7.2	10.8	40	49	11
QS-2/3 Top	30.3	8.3	7.1	7.7	6.8	4.5	35.2	30	35	35
QS-4	51.0	5.5	5.5	3.8	6.0	3.6	24.8	51	24	25
QS-5	19.1	3.3	4.3	8.3	10.9	6.9	47.2	19	34	47
QS-6	8.8	2.6	5.8	4.0	6.9	5.5	66.4	9	25	66
QC-1.1	5.0	2.0	8.0	14.0	31.0	10.0	30.0	5	65	30
QC-1.2	25.0	4.0	4.9	5.2	3.0	9.1	48.8	25	26	49
QC-2	7.1	7.5	2.8	10.3	7.1	12.6	52.6	7	40	52
QC-3	2.6	1.3	2.6	8.2	3.6	7.6	74.0	3	24	74
QC-4	6.4	3.0	4.9	2.6	13.5	14.3	55.3	6	38	55
QC-5 Base	14.3	3.3	7.2	12.5	14.3	9.0	39.4	14	46	39
QC-6 Base	18.1	4.4	9.9	8.5	4.1	8.5	46.5	18	35	46

Values are expressed in %.

aggregates (Fig. 5C).

The QC-5 mineral assemblage varies significantly from the base to the top of the unit. Calcite content increases from the base (30%) to the top (52%), whereas quartz content nearly halves (30–17%) and clay minerals decrease (22–13%). The remaining minerals appear in smaller and similar quantities (Table 2). The texture of the QC-5 unit is detritic, composed of calcite and quartz clasts, alongside aluminum-rich (smectite) and magnesium-rich (palygorskite) clays. EDS analyses reveal phosphate-rich, calcium-rich masses, indicating the presence of guano deposits in the level.

Calcite (48–52%, mean = 50%), quartz (20–23%, mean = 21.5%), clay minerals (14–15%, mean = 14.5%), and dolomite-ankerite (5–12%, mean = 8.5%) are the main mineral constituents of unit QC-6, with minor quantities of plagioclase, K feldspar, goethite, hematite, and apatite (Table 3).

4.2.2. *Quibas-Sima section*

Calcite (14–48%, mean = 34.2%), quartz (15–33%, mean = 23.3%), clay minerals (14–23%, mean = 16.8%), and dolomite-ankerite (5–27%, mean = 16.5%) are the most abundant minerals in QS-1 levels (Table 2). Both organic-matter-rich levels (QS-1.1 OMR and QS-1.2 OMR) contain lower quantities of calcite (14 and 22%, respectively) and, alongside the

Table 2
XRD results for the studied samples from the Quibas site showing the Reference Intensity Ratios (RIR) of the existing phases, allowing the intensity calculations to be normalised on the assumption that the sum of all phases in the sample is equal to 100%.

Sample	Quartz	Clay minerals	Plagioclase	K feldspar	Calcite	Aragonite	Dolomite-Ankerite	Goethite	Hematite	Apatite	Halite	Gypsum
QS-6	34	25	3	4	17	8	5	1	1	1	–	1
QS-5 Top	20	15	2	3	46	2	10	–	–	–	1	1
QS-5 Base	28	13	2	4	32	–	19	–	–	–	1	1
QS-4 Top	13	7	–	5	60	–	11	–	–	–	3	1
QS-4 Base	13	9	–	5	60	1	10	–	–	–	1	1
QS-3	12	9	–	2	45	2	29	–	1	–	–	–
QS-2/3	17	13	1	3	46	1	18	–	1	–	–	–
QS-2	14	13	1	3	44	–	25	–	–	–	–	–
QS-1.3	20	15	1	3	48	1	12	–	–	–	–	–
QS-1.2	20	15	1	3	37	2	19	–	1	2	–	–
QS-1.2 OMR	23	15	2	4	22	2	27	1	1	3	–	–
QS-1.1 Top	23	19	2	4	45	1	5	1	–	–	–	–
QS-1.1 OMR	33	23	3	4	14	1	18	1	–	3	–	–
QS-1.1 Base	15	14	2	2	39	2	18	–	1	7	–	–
QC-6 Top	20	14	1	3	48	–	12	–	1	1	–	–
QC-6 Base	23	15	1	3	52	–	5	1	–	–	–	–
QC-5 Top	17	13	2	4	52	1	9	–	1	1	–	–
QC-5 Base	30	22	2	5	30	1	7	1	1	1	–	–
QC-4	30	30	2	7	18	1	8	1	1	2	–	–
QC-3	25	14	2	4	33	2	18	–	1	1	–	–
QC-2	19	14	1	3	28	–	31	1	1	1	1	–
QC-1.2	21	18	1	4	37	–	17	–	1	1	–	–
QC-1.1	22	21	2	4	34	4	11	–	1	1	–	–

Table 3
Anion and cation results of the Quibas samples with an electrical conductivity value ≥ 4 dSm^{-1}.

Sample	Cl^- (mg/L)	NO^{3-} (mg/L)	SO_4^{2-}(mg/L)	Ca^{2+} (318,127 nm) ppm	Na^+ (589,592 nm) ppm
QS-1.2 OMR	212.75	242.5	166.39	226.61	554.98
QS-4 Base	1922.5	42.13	221.82	112.7	650.05
QS-4 Top	69.99	946.8	15.42	143.04	974.51
QS-5 Base	1749.71	30.49	385.56	118.02	668.04
QS-5 Top	1384.62	26.13	210.49	119.79	402.27

fossil-rich levels QS-1.2 and lowermost QS-1.1 (QS-1.1 Base), significant quantities of apatite (Table 2). SEM observations reveal levels QS-1.1, QS-1.1 OMR, QS-1.2 OMR and QS-1.3 are very porous, with abundant micrite and palygorskite (Fig. 6A and B). Euhedral rhombic dolomite-ankerite crystals appear crystallized on top of other minerals, with only dense fibrous palygorskite masses growing as bridges on and between them (Fig. 6C). On the other hand, level QS-1.2, although mineralogically very similar to QS-1 levels, is texturally very different, being less porous, more detritic and with allochthonous quartz, feldspar, and calcite rounded and sub-rounded clasts (Fig. 5D).

The muddy sand matrix of unit QS-2/3 is mainly composed of calcite (44–46%, mean = 45%) and dolomite-ankerite (18–29%, mean = 24%), followed by much lower quantities of quartz and clay minerals and traces of plagioclase, alkali feldspars, and hematite (Table 2). When observed under the SEM, QS-2/3 levels are very detritic, with abundant calcite and dolomite-ankerite sub-rounded and sub-angular clasts.

Muddy sands in QS-4 are composed of calcite (60%), quartz (13%), and dolomite-ankerite (10–11%), with low quantities of clay minerals (7–9%) and alkali feldspars (5%). Unit QS-4 has a high content of salts ($\geq$4 ds/m), with high chloride and sulphate anions values, while the most abundant cations are calcium and sodium. This is a clear indication of the presence of halite (sodium chloride) and gypsum (calcium sulphate) salts (Table 3). For the first time in the Quibas-Sima section, halite (1–3%) and gypsum (1%) are present (Table 2). SEM observations show calcite crystals overgrown by calcite and dolomite-ankerite crystals.

Calcite (32–46%, mean = 39%), quartz (20–28%, mean = 24%), dolomite-ankerite (10–19%, mean = 14.5%) and clay minerals (13–15%, mean = 14%) are the most abundant minerals in unit QS-5, alongside small quantities (<5%) of plagioclase, alkali feldspars, halite, and gypsum (Table 2). The clastic texture of QS-5, observable under a SEM, is composed mainly of calcite, quartz, and dolomite-ankerite sub-rounded clasts in a clayey matrix, with palygorskite and salts (halite and gypsum) growing on pore walls and as aggregates on clasts and crystals.

The muddy sand matrix of unit QS-6 is composed of quartz (34%), clay minerals (25%), and calcite (17%), with some accessory minerals such as plagioclase, alkali feldspars, aragonite, dolomite-ankerite, goethite, hematite, apatite, and gypsum (Table 2). Abundant bioturbation pores affecting the clastic texture of the sample can be observed under the SEM.

5. Discussion

5.1. Sedimentary facies, depositional environments, and stratigraphic correlations

Previous studies have classically divided karst deposits into three main groups: allochthonous, autochthonous, and chemical deposits (e.g. Ford and Williams, 2007; White, 2007b). In this study, chemical deposits are assumed to be autochthonous. Furthermore, Bosch and White (2018) divide clastic sediment facies in caves into five types: backswamp facies, channel facies, diamicton facies, slackwater facies, and thalweg facies. Quibas site hosts a wide variety of these karstic facies, which will be discussed below.

5.1.1. Channel facies

Channel facies are allochthonous, and are considered the underground equivalent (in vadose conditions) of stream deposits on the surface (Bosch and White, 2018). These facies are very variable, including crudely bedded to massive deposits, ranging from unbedded to horizontal bedding or ripple crossbedding. Several channel facies are recognized at the Quibas site: QC-1.1, QC-2, and the lowermost part of QS-1.1. These units host well-sorted gravelly deposits containing both angular and sub-angular limestone and speleothem clasts in muddy or

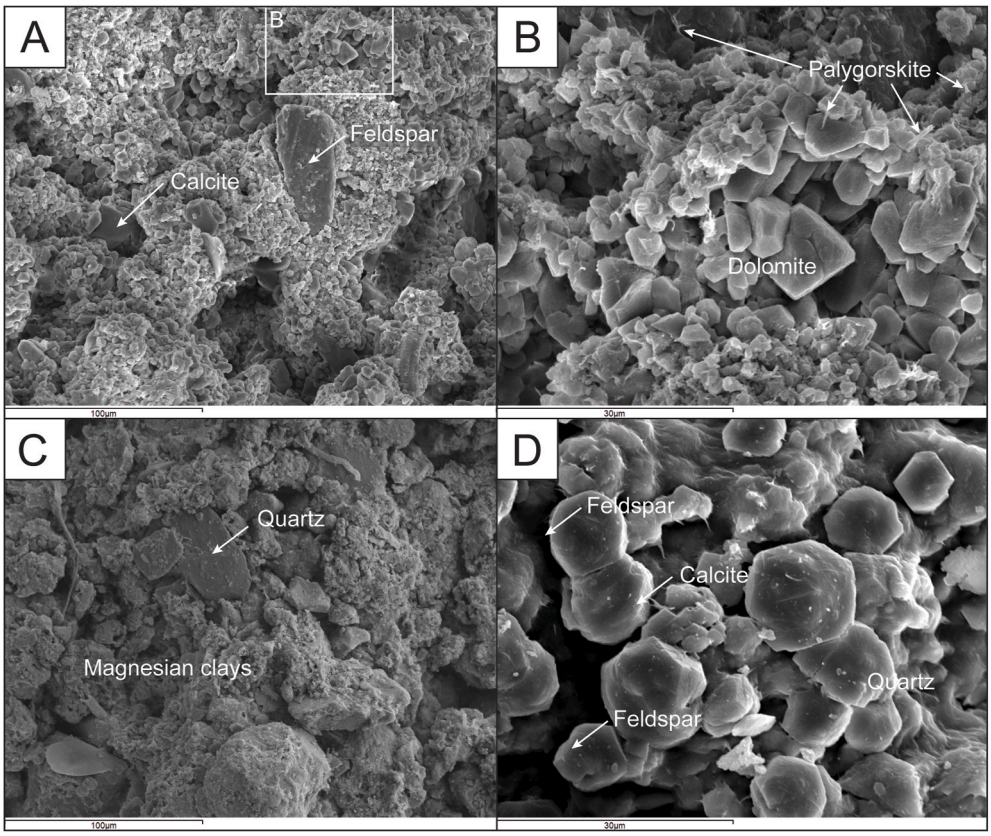

Fig. 5. SEM images of representative sample chips. A. Unit QC-1.2. Sub-angular and sub-rounded calcite clasts with high sphericity, alongside bigger, less spherical, and more angular calcite, quartz, and feldspar clasts. B. Unit QC-1.2. Euhedral rhombic dolomite-ankerite crystals growing on pore walls, with palygorskite fibres as bridges on and between clasts and crystals. C. Unit QC-4. Allochthonous quartz, feldspar, and calcite angular and sub-angular, low-sphericity clasts with abundant magnesian clay aggregates. D. Unit QS-1.2. Allochthonous quartz, feldspar, and calcite rounded and sub-rounded clasts.

sandy matrices. SEM observations reveal that channel facies exhibit similar textural properties, with clastic textures where abundant sun-angular to sub-rounded allochthonous clasts are found alongside bigger, less spherical, and more angular autochthonous clasts (Fig. 5A).

The presence of root bioturbation and polyhedral aggregates in unit QC-2 indicates an open cave environment where an entrance to the cave would be located nearby.

5.1.2. Backswamp facies

Backswamp facies is a term used to refer to the leftover material from bedrock dissolution, which was filtered from the epikarst (Bosch and White, 2018). The mineralogical composition of these facies depends mainly on the composition of the insoluble fraction of the calcareous bedrock. These facies usually display a massive structure and may contain isolated clast fragments and fossils.

Lithostratigraphic units QC-4, QS-1.1 and QS-1.3 are interpreted as backswamp facies. These units are very muddy (40–80% mud; Fig. 4), massive, and contain scarce limestone megaclasts and boulders, product of cave breakdown. All three units also host abundant microvertebrate remains, with high-density bone accumulations in unit QC-4 and two fossil- and organic-rich levels in unit QS-1.1.

The stratigraphic positions and facies suggest units QC-4 and QS-1.1 can be correlated (Fig. 7). The presence of polyhedral aggregates in QC-4 and abundant root bioturbation in QS-1.3 indicates these units were deposited in an open cave environment with a nearby open cave entrance.

5.1.3. Underground debris flow facies

The underground equivalent to debris flows in karstic systems are diamicton facies, in which materials of all particle sizes and morphologies are suspended and flow down high-gradient passages or sub-vertical entries (Bosch and White, 2018).

QC-1.2, QC-3, QC-5, and QS-1.2 deposits are chaotic, unsorted, unbedded, massive, and interpreted as diamicton deposits. QC-1.2, QC-3, and QC-5 are poorly sorted breccias and megabreccias, with angular limestone and speleothem clasts with textures varying from matrix-supported to clast-supported with a scarce matrix. These three units represent proximal diamicton facies close to the inferred paleoentrance: a high-gradient (45–60°) north-dipping passage towards the south. The deposition of unit QC-5 completely infills and blocks this paleoentrance. The poorly sorted, polymodal gravelly mud deposits of unit QS-1.2 represent the distal facies of the QC-5 diamicton deposits.

SEM observations reveal a clastic texture, with unsorted sub-angular and sub-rounded calcite, quartz, and feldspar clasts (Fig. 5A).

5.1.4. Debris flow facies

Debris flows are high-density, one-phase clastic flows (Coussot and Meunier, 1996; Dasgupta, 2003). Debris flows commonly show no bedding and are formed by a chaotic mixture of clast sizes, ranging from clay to boulders (Coussot and Meunier, 1996; Dasgupta, 2003). In this study, debris flow facies and diamicton facies are separated according to their depositional environment: the former in open-air environments (e.g. dolines or avens), whereas the latter in a closed-cave environment (e.g. cave chambers or galleries).

Debris flow facies are found in both sections of the Quibas site: unit QC-6 in Quibas-Cueva and unit QS-2/3 in Quibas-Sima. These two units can be correlated laterally (Fig. 7). The gravelly mud-rich deposits of unit QC-6 are interpreted as distal facies, while the breccia deposits of unit QS-2/3 constitute the proximal facies of the same debris cone. This unit marks a shift in the depositional environment, from a karstic system

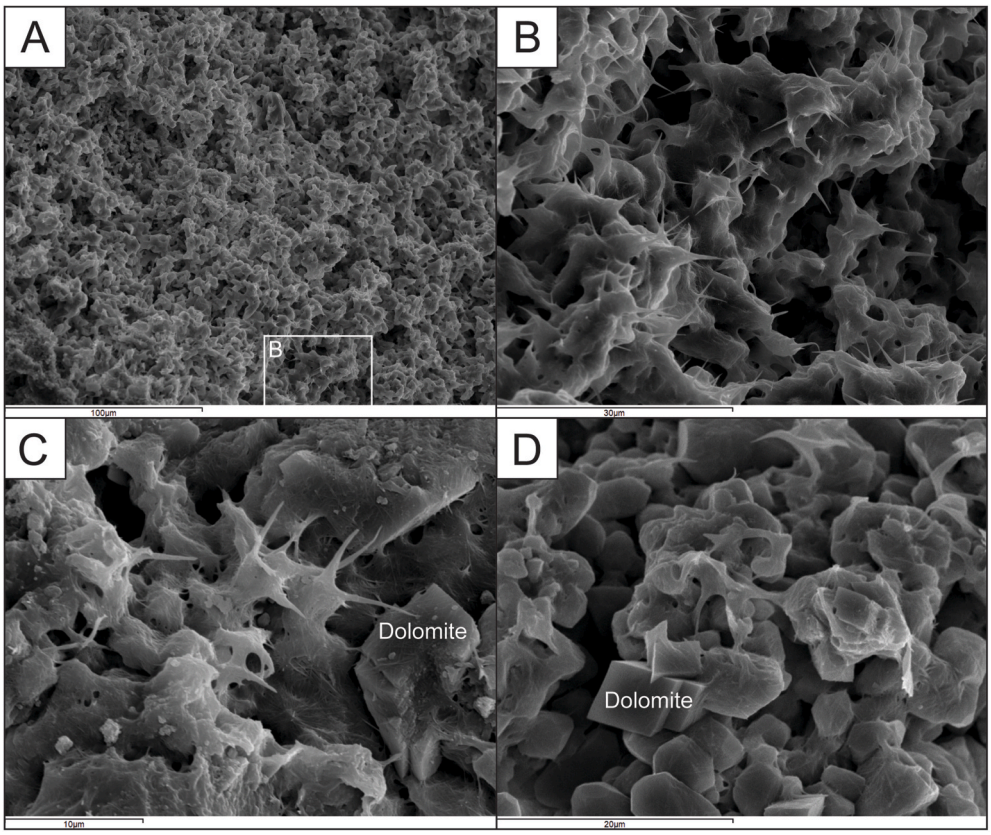

Fig. 6. SEM images of representative sample chips. A. Unit QS-1.1 general texture. Very porous, with micrite and palygorskite. B and C. Unit QS-1.1 detailed images, showing abundant palygorskite fibres. D. Unit QC-3. Euhedral rhombic dolomite-ankerite crystals crystallized on top of other minerals, with dense fibrous palygorskite masses growing as bridges on and between them.

to an open-air environment, with the formation of a new overhead opening or aven.

5.1.5. Debris fall facies

Debris fall facies are characterized by sedimentary deposits that have fallen under gravity where no interstitial fluid is necessary. These deposits consist of heterometric clast accumulations, typically angular, with little or no matrix (open-work to clast-supported), with crude lateral sorting and commonly normal or inverse crude grading. These deposits are associated with sub-vertical and vertical cave entrances, cliffs, and steep slopes.

The clast-supported heterometric breccias with normal and inverse crude grading of units QS-4 and QS-7 and the clast-supported microstratified breccia of unit QS-5 have been interpreted as debris fall deposits (Fig. 3). Clasts are angular and chiefly composed of limestone and speleothem fragments from wall and roof breakdown. Additionally, at least seven rockfall events have been identified in the Quibas site: at the base of unit QC-1.1, embedded in diamicton deposits of units QC-1.2 and QC-5, and during the deposition of unit QS-2/3 (Figs. 2 and 3). These rock fall deposits indicate events of cave walls and roof dismantling.

5.1.6. Paleosol facies

Sandy mud deposits formed either by the dissolution of the host rock (weathering detritus, White, 2007a) or by colluvial processes that have suffered pedogenic processes are classified as authochthonous paleosol facies.

The matrix-supported and microstratified colluvial breccias of units QS-5 and QS-6 with muddy sand matrices, heavily altered by pedogenic processes, are interpreted as paleosol (argillic leached horizon). Caliche development, in the form of laminar crusts and hardpans (Wright and Tucker, 1991), is observed in the contact between units QS-4 and QS-5 and towards the top of unit QS-5 (Fig. 3).

5.1.7. Speleothems and phosphatic accumulations

Chemical sediments in caves are formed via precipitation of different chemical substances. The main two chemical facies in the Quibas site are speleothem formations (flowstones) and phosphatic accumulations.

The Quibas site has two well-developed flowstones, S1 and S2. The lower S1 flowstone, embedded in unit QS-1.3, is laminar and laterally discontinuous. On the other hand, the upper S2 flowstone is thicker and polygenetic, composed of laminar, coralloid, and massive speleothem formations. The S2 flowstone overlies unit QS-1.3 in the Quibas-Sima section and can be traced laterally to overlie QC-5 in the Quibas-Cueva section (Figs. 2 and 3).

Units QS-2/3 and QC-5 contain millimeter-to-centimeter-thick yellowish phosphatic passings with little lateral continuity. Additionally, EDS analyses of unit QC-5 reveal phosphate-rich, calcium-rich masses. These phosphate deposits are interpreted as bird and bat guano (Weiner et al., 2002; Shahack-Gross et al., 2004).

5.2. Paleoclimatic inferences

Two distinct paleoclimatic signals, discussed below, can be distinguished in both the Quibas-Cueva and Quibas-Sima sections. These have enabled the identification of several alternating humid and arid phases derived from the Early Pleistocene glacial-interglacial cycles.

5.2.1. Pre-Jaramillo warm and humid period

The lowermost section of the Quibas paleontological sections (Quibas-Cueva and Quibas-Sima), comprising units QC-1 to QC-5 and QS-1.1 to QS-1.3, hosts a wide array of clay-rich, water-lain karstic deposits, as well as the development of two flowstones (S1 and S2) (Figs. 8 and 9).

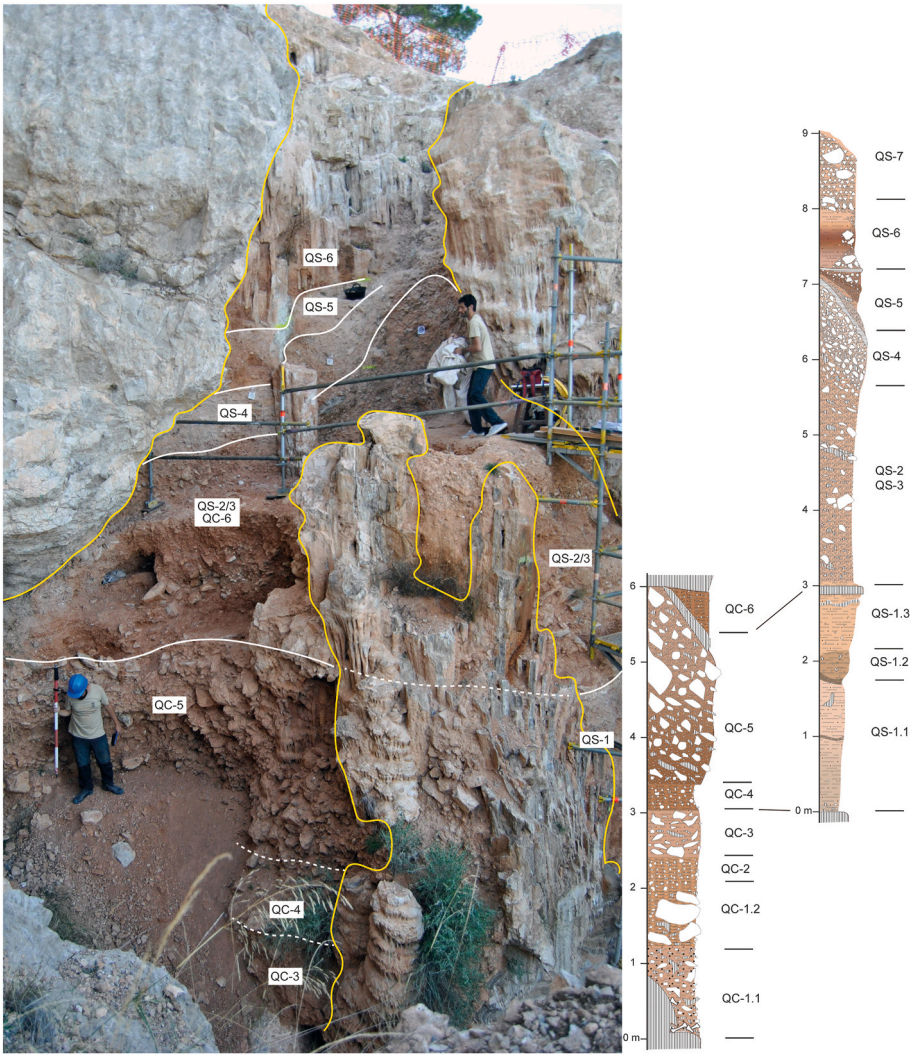

Fig. 7. Stratigraphic correlation between Quibas-Cueva and Quibas-Sima lithostratigraphic units. Legend as in Figs. 2 and 3.

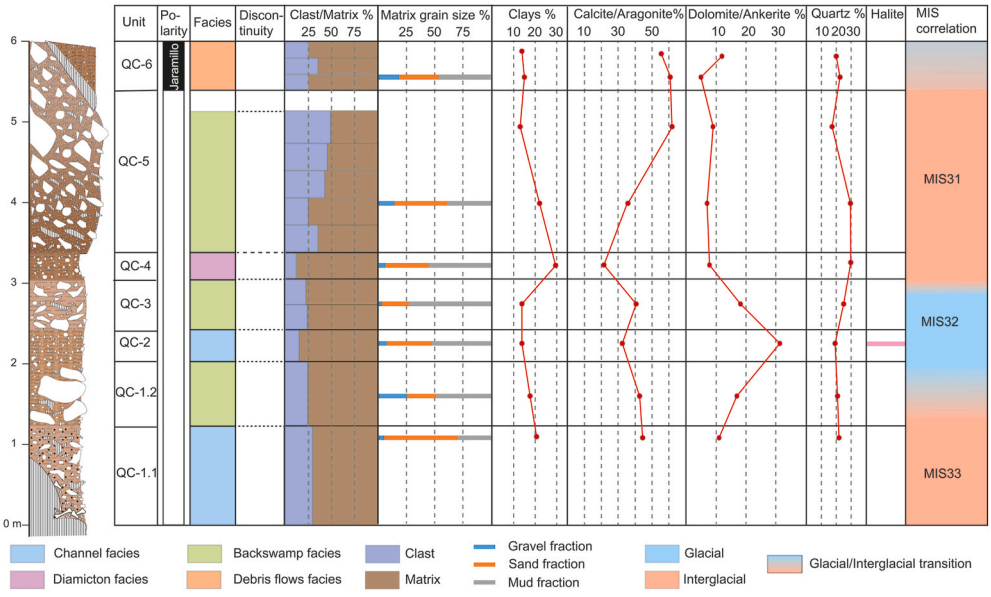

Fig. 8. Summary table of principal analyses conducted in the Quibas-Cueva section, identified facies, and probable Marine Isotope Stage (MIS) correlation. Paleomagnetic data is sourced from Piñero et al. (2020, 2022).

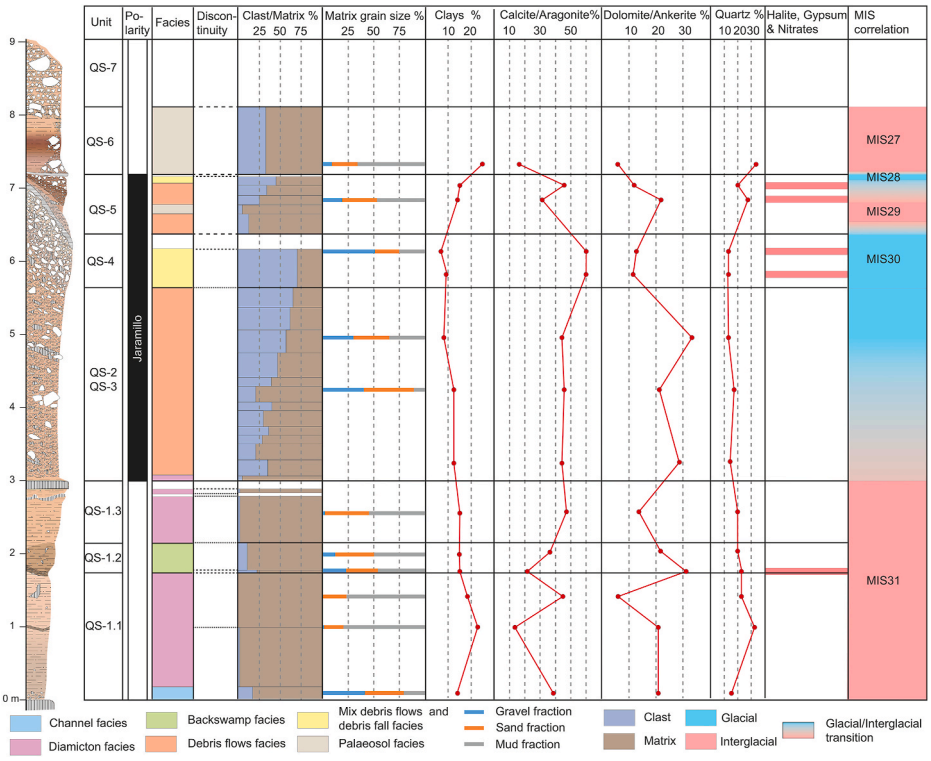

Fig. 9. Summary table of principal analyses conducted in the Quibas-Sima section, identified facies, and probable Marine Isotope Stage (MIS) correlation. Paleomagnetic data is sourced from Piñero et al. (2020, 2022).

Water-lain karstic deposits, including channel facies (units QC-1.1, QC-2, and lowermost QS-1.1), diamicton facies (units QC-1.2, QC-3, QC-5, and QS-1.2), and backswamp facies (QC-4, QS-1.1, and QS-1.3) (Figs. 8 and 9) are indicative of a constant hydric regime inside the karstic system, which can also be related to hydric processes at a regional scale (Hunt et al., 2010; Wagner et al., 2011). Although this does not necessarily indicate humid conditions, the presence of concave and irregular basal contacts, alongside scour structures, does indicate that water is abundant in the karstic system and flooding events are common (Bosch and White, 2018). On the other hand, speleothem precipitation (S1 and S2) indicates higher precipitation rates than evaporation-runoff rates (Bar-Matthews, 2014), which hinders precipitation in semi-arid conditions and completely prevents it in arid/hyper-arid deserts. Therefore, it does suggests formation during humid conditions (Fleitmann et al., 2003; Vaks et al., 2003, 2007) (Fig. 8).

The presence of halite in unit QC-2 could suggest that this unit was deposited during a relatively dry period with high evaporation rates (Gornitz, 2009) (Fig. 8). Palygorskite is widely accepted as a paleoclimatic indicator of semi-arid to arid environments (Singer and Norrish, 1974; Weaver and Beck, 1977; Singer, 1984; Hong et al., 2007; Galán, 2011; Knidiri et al., 2014; Hill et al., 2017). However, recent studies have stated only detrital palygorskite, originated as catchment-delivered detritus, should be used in paleoclimate reconstructions, whereas authigenic palygorskite that has formed during post-depositional processes should not be used (Ye et al., 2018). Fibrous palygorskite masses growing as bridges on and between all other clasts are observed in units QC-1.1, QC-1.2, QC-3, QC-5 and QS-1 (Fig. 5). These textures suggest an authigenic origin attributed to direct precipitation during diagenesis (Hong et al., 2007) and, therefore, cannot be used as a paleoclimatic indicator.

The Quibas-Sima section records a polarity change from a reverse interval (QS-1) to a normal one (QS-2/3, QS-4, QS-5), followed by a second reverse one (QS-6 and QS-7). This normal polarity interval bounded by reverse polarities is identified as the Jaramillo subchron. The base of Quibas-Cueva (QC-1 to QC-5) showed a reverse polarity, which was correlated with the reversed interval recorded at base of Quibas-Sima (Piñero et al., 2020, 2022). This paleomagnetic study places the deposition of units QC-1 to QC-5 and QS-1 sometime between the Punaruu and Jaramillo subchrons (between 1.12 and 1.07 Ma), during Marine Isotopic Stages (MIS) 31–33 (Figs. 8 and 9). The entire interval from MIS 33 to 31 has been identified as one warm, long-lasting interglacial (DeConto et al., 2007; Teitler et al., 2007; de Wet et al., 2016). In the central and western Mediterranean region, MIS 31 has been described as a warm, temperate, and very humid period with weak seasonality (Joannin, et al., 2011; Oliveira et al., 2017). The paleoclimatic inferences proposed in this study for this lowermost section of the Quibas site agree with such a warm, humid interglacial (Fig. 10).

In this "super interglacial scenario" (DeConto et al., 2007; Teitler et al., 2007; de Wet et al., 2016), MIS 32 would be reduced to a stadial. Given that unit QC-2 was deposited during a drier period, it is possible that this unit was formed during this colder, drier stadial (1.104–1.081 Ma). This would further delimit the inferred geochronology of the pre-Jaramillo units: units QC-1.1 and QC-1.2 during MIS 33 (1.114–1.104 Ma), and QC-3 to QC-5 and QS-1.1 to QS-1.3 sometime during MIS 31 (1.081–1.062 Ma) before the Jaramillo subchron (Fig. 10).

5.2.2. *Jaramillo and post-Jaramillo arid period*

Units QC-6 and QS-2/3 to QS-5 correspond to a normal polarity interval, identified as the Jaramillo subchron (Piñero et al., 2020, 2022). These units, when compared to the lower pre-Jaramillo deposits, exhibit a progressive decrease in clay mineral and quartz content and an increase in the clast-to-matrix ratio (Figs. 8 and 9). Assuming that the entry point through which the sediments enter is a vertical fissure (aven) in a zenithal position, transport is inferred to be minimal. For this reason, this trend observed in mineral fractions and matrix versus clast content must be controlled by sediment production in the source area. This implies a decrease in chemical weathering and an increase in mechanical weathering due to a decrease in the precipitation regime and an

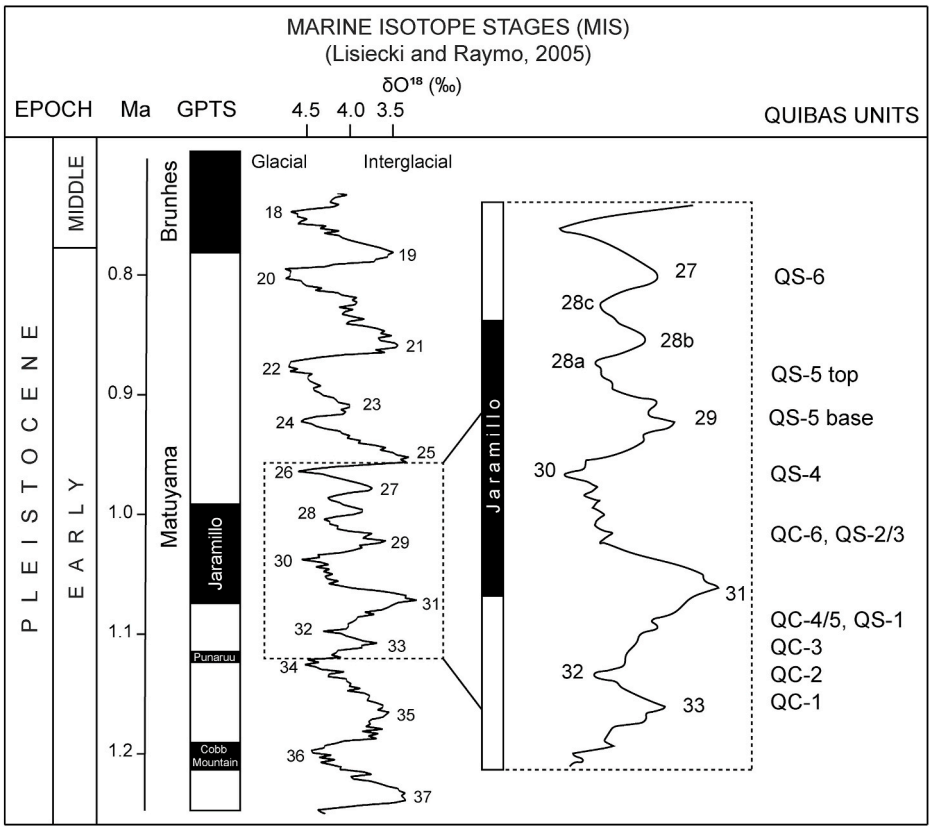

Fig. 10. Chronological position of the different units of Quibas-Cueva and Quibas-Sima (Piñero et al., 2020, 2022) and their correlation with Marine Isotope Stages (MIS). GPTS (Geomagnetic Polarity Time Scale) shows Bruhnes and three normal polarity intervals within Matuyama: Jaramillo (1.07–0.99 Ma), Punaruu (1.12 Ma), and Cobb Mountain (1.22–1.19 Ma) (Singer, 2014).

increase in aridity. This increase in climate aridity is also supported by paleontological data (Piñero et al., 2020, 2022), as discussed below. The progressive increase in aridity is consistent with a transitional period between an interglacial phase and a glacial phase, corresponding to MIS 31 and MIS 30, respectively, according to the chronological framework (Fig. 10).

Unit QS-4 has the lowest clay mineral and quartz content and the highest clast/matrix ratio, coupled with a high concentration of calcium carbonate and lower amounts of dolomite (Figs. 8 and 9). This is consistent with an arid climate, as a decrease in precipitation leads to a decline in chemical weathering, consequently resulting in a lower generation of insoluble residue (clay minerals and quartz) from carbonate dissolution. Furthermore, according to the results of the electrical conductivity, unit QS-4 has a high content of salts ($\geq$4 dSm^{-1}) (Table 3). A more significant precipitation of salts explains the significantly higher abundance of gypsum and halite in unit QS-4 concerning the rest of the levels, which could be related to periods of aridity. The dolocrete at the top of this unit also supports the interpretation of an arid environment with scarce vegetation and low sedimentation rates. This arid period can be correlated to the glacial MIS 30 (Fig. 10).

In unit QS-5, the facies suggest a re-establishment of relatively humid and warm conditions compared to the previous unit QS-4. The hypothesis is supported by the presence of debris flow layers and paleosol horizons. The unit still falls within the normal polarity assigned to the Jaramillo subchron and may represent the following interglacial period, represented by MIS 29. At the top of this unit, the presence of halite, gypsum, and nitrates, along with the presence of a new caliche/calcrete horizon, indicates a return to more arid conditions and could be correlated with the subsequent glacial episode, represented by MIS 28. The thicker paleosol in unit QS-6, which overlies the calcrete/caliche of QS-5, suggests a new return to humid conditions. The reverse polarity of this unit indicates the Jaramillo-end inversion, suggesting it may represent interglacial MIS 27 (Fig. 10). Unfortunately, no vertebrate remains have been found in QS-5 and QS-6 to corroborate this assumption.

5.2.3. *Paleontological record*

The Early Pleistocene glacial episodes in Europe led to an increase in aridity, resulting in the expansion of open areas. Conversely, during interglacial phases, precipitation levels rose, leading to the spread of forested areas (Leroy et al., 2011). The mineralogical composition of the different units of Quibas offers evidence of a transition from moist interglacial conditions (QC-4, QC-5, QS-1) to arid glacial conditions (QS-2/3, QS-4). These findings are consistent with the small vertebrate succession identified in QS-1 to QS-4 (Piñero et al., 2022). The oldest of these units, QS-1, has yielded fossils of a flying squirrel from the *Hylopetes* genus, a rodent typically associated with forested environments (e.g. Lee, 2016). QS-1 also contains remains of the water shrew *Neomys* sp., a semi-aquatic insectivore, indicating the existence of stable water courses in the vicinity of Quibas at the time of sediment deposition (Palomo and Gisbert, 2002). Furthermore, QS-1 is correlated with QC-4 and QC-5, units recording the presence of the legless lizard *Ophisaurus manchenioi*, a reptile whose extant relatives inhabit tropical and subtropical regions (Blain and Bailon, 2019). Its presence in Quibas verifies that the southeastern part of the Iberian Peninsula served as the last refuge for subtropical species in Europe. The presence of these species in the earliest units of the site suggests that forests thrived under relatively humid conditions during their formation.

Nevertheless, *Neomys* sp. and *Ophisaurus manchenioi* disappear from the lower part of QS-2/3, and *Hylopetes* sp. from the upper part of this unit. This corresponds to the presumed loss of habitat suitable for the survival of these species during the deposition of this unit. Conversely, QS-3 and QS-4 have yielded fossils of reptiles associated with open and

scrub environments, including the Montpellier snake (*Malpolon monspessulanus*) and the snub-nosed viper (*Vipera latastei*) (Pleguezuelos, 1997; Pleguezuelos and Santos, 2004), species absent in QS-1 (Piñero et al., 2020). Similar to the mineralogical composition, the ecological preferences of the small vertebrates in Quibas-Sima illustrate a record of climate change. This change shift from forested and humid conditions in the earliest part (QS-1) to drier conditions, marked by greater expanses of open scrubland, in the more recent levels (QS-2/3 to QS-4).

Thus, the data aligns with the onset of a glacial phase about 1 Ma, characterized by an increase in aridity and, consequently, a decrease in tree cover in the southeastern region of Iberia. This environmental change coincided with the transition from the MIS 31 interglacial to the MIS 30 glacial during the Jaramillo subchron.

5.3. Geological evolution and synthesis

A rough reconstruction of the development of the cave can be inferred from its morphology and fills (Fig. 11). The bedrock underwent dissolution, favored along pre-existing faults, during the Miocene to Pliocene (Rodríguez Estrella et al., 2004) (Fig. 11A). This potentially hypogenic phreatic stage probably ended at the end of the Pliocene. The almost horizontal nature of the cave suggests that it formed close to the phreatic level, at least during its later stages of development. This is followed by a vadose stage, during which an active karst system developed before sediment deposition (Late Pliocene and Early Pleistocene) (Fig. 11B). The first entrance of the cave system was formed during the Early Pleistocene. The opening of the cave to the outside is marked by the formation of a cemented limestone breccia on the floor of the cavity containing macrofaunal remains. Although it is possibly earlier, this unit is in continuity with a large cemented and fossilized landslide with speleothems, within which remains of macro- and microfauna are also found (Piñero et al., 2015). The rest of the Quibas-Cueva and Quibas-Sima units are deposited on top of this basal unit (Fig. 11C). The units beneath the roof of speleothem S2 correspond to the pre-Jaramillo reverse period. They have karstic facies and were deposited during a warm and humid period correlated with the MIS 33–31 super interglacial event (Fig. 11D). The formation of speleothems S1 and S2 would correspond to the closing event of the first cave entrance and the re-establishment of a closed cave environment (Fig. 11E and F). Above speleothem S2, the opening of a chasm in the zenithal part of the cave triggered the deposition of debris flow facies in an alluvial cone, depositing unit QS-2/3 (Fig. 11G). This unit represents a transition between the previous humid period and the arid period represented by unit QS-4, corresponding to the glacial period of MIS 30 (Fig. 11H). Unit QS-5 shows a return to a relatively humid period at its base and becomes arid towards the top, representing the end of the Jaramillo subchron. Unit QS-6 is of normal polarity, represented by paleosol facies, corresponding to a wetter period right after the Jaramillo subchron (Fig. 11I).

Summarizing, in the paleontological site of Quibas, at least two main entrances have been identified. The first corresponds to the main cave entrance, which, due to successive collapses, would have shifted to a closer position. Subsequently, this entrance would have been sealed by a cone of debris (diamicton facies), and the cave would have returned to a closed environment. The second entrance corresponds to the opening of a shaft in the upper part of the cave, which would have culminated in its infilling.

6. Conclusions

The Quibas site has functioned as a sediment trap since its opening to the outside in the Early Pleistocene, until the cave filled up. During this time, the cave has been infilled mainly by clastic sediment containing macro- and microfaunal paleontological remains.

Seven different facies types have been identified throughout the different lithostratigraphic units of Quibas: 1) channel facies in units QC-1.1, QC-2, and the lowermost part of QS-1.1; 2) backswamp facies in units QC-4, QS-1.1, and QS-1; 3) diamicton facies in units QC-1.2, QC-3, QC-5, and QS-1.2; 4) speleothem facies, consisting of two well-developed flowstones, embedded in unit QS-1.3 (S1), and overlying unit QS-1.3 and unit QC-5 (S2); 5) debris flow facies in units QC-6, QS-2/3, QS-4, and part of unit QS-5; 6) debris fall and rock fall facies in QS-7, at the base of unit QC-1.1, embedded in diamicton deposits of units QC-1.2 and QC-5, and during the deposition of unit QS-2/3; and 7) paleosol facies in units QS-5 and QS-6.

Two distinct paleoclimatic signals can be distinguished in both the Quibas-Cueva and Quibas-Sima sections, which have enabled the identification of up to seven alternating humid and arid phases resulting

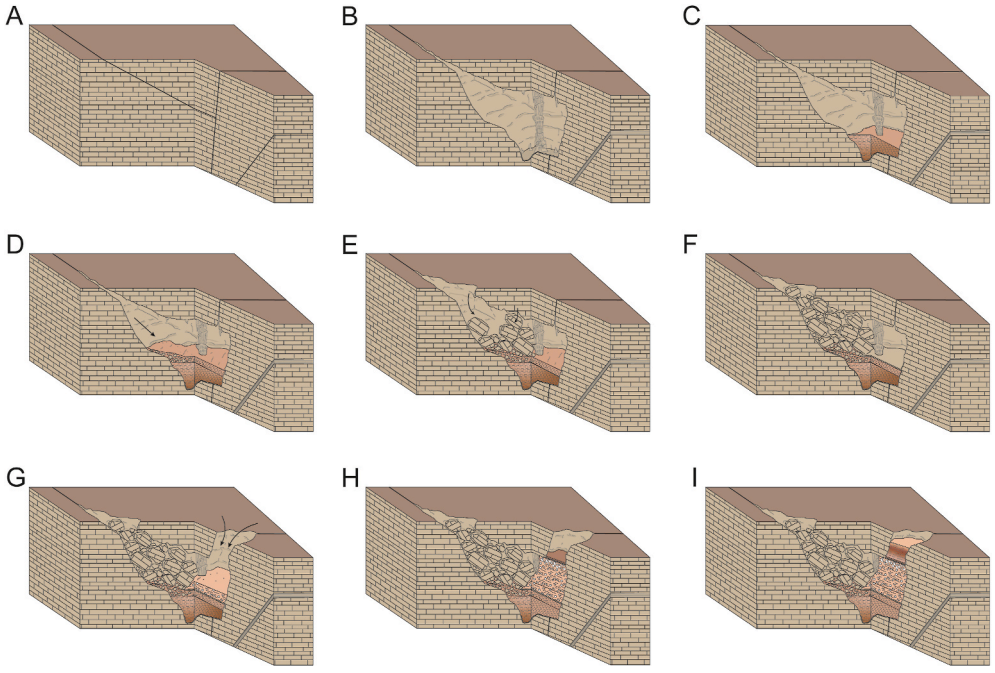

Fig. 11. Geological evolution and synthesis of Quibas site.

from the Early Pleistocene glacial/interglacial dynamics. The high-precision chronology of the Quibas site has allowed the correlation of the detected paleoenvironmental shifts to the marine oxygen isotope record.

The lowermost pre-Jaramillo units (QC-1 to QC-5 and QS-1.1 to QS-1.3) suggest these were deposited during a warm, humid period, correlated to the interglacial MIS 33–31. The Jaramillo units QS-2/3 and QC-6 indicate deposition during a period of increasing aridity up to a period of maximum aridity represented by unit QS-4, correlated to the glacial MIS 30. The Jaramillo unit QS-5 and the post-Jaramillo unit QS-6 suggest these were deposited in alternating periods of aridity and humid conditions, although less humid than the pre-Jaramillo period, probably representing the interglacial MIS 29, glacial MIS 28 and interglacial MIS 27.

Data availability

The authors confirm that all the data supporting the findings of this study are available within the article.

CRediT authorship contribution statement

Casto Laborda-López: Conceptualization, Methodology, Formal analysis, Data curation, Investigation, Visualization, Validation, Supervision, Writing – original draft. **David M. Martín-Perea:** Conceptualization, Methodology, Formal analysis, Data curation, Investigation, Visualization, Validation, Supervision, Writing – original draft. **Elia Del Castillo:** Methodology, Formal analysis. **M. Asunción Alías Linares:** Methodology, Formal analysis, Investigation, Writing – review & editing. **Claudia Iannicelli:** Methodology, Writing – review & editing. **Shubham Pal:** Methodology, Writing – review & editing. **Xabier Arroyo:** Methodology, Formal analysis. **Jordi Agustí:** Resources, Validation, Project administration, Funding acquisition, Writing – review & editing, Visualization. **Pedro Piñero:** Resources, Validation, Project administration, Funding acquisition, Writing – original draft, Writing – review & editing, Visualization.

Declaration of competing interest

The authors declare that they have no known competing financial interests or personal relationships that could have appeared to influence the work reported in this paper.

Acknowledgements

This work was supported by the Spanish Ministry of Science and Innovation [grant number PID 2021-123092NB-C21], AGAUR-Generalitat de Catalunya [grant number 2021SGR-1238], and University Rovira i Virgili [grant number 2023PFR-URV-01238]. The IPHES-CERCA has received financial support from the Spanish Ministry of Science and Innovation through the “María de Maeztu” program for Units of Excellence [grant number CEX 2019-000945-M]. DMMP was funded by the European Union - NextGenerationEU. PP is supported by a “Juan de la Cierva-Incorporación” contract [grant number IJC 2020-044108-I] funded by MCIN/AEI/10.13039/501100011033 and “European Union NextGenerationEU/PRTR”. We would like to express our gratitude to José Antonio Blasco, Manuel Carlos Cutillas, and the Abanilla City Council for the financial and logistical support provided to the Quibas excavation team during the different field campaigns. We wish to extend our thanks to José Francisco Lajara, Gregorio Romero, and the Dirección General de Patrimonio Cultural of the Region of Murcia for their support in conducting this research. We are also grateful to Julio Aguirre and Angel Puga from the Department of Stratigraphy and Palaeontology at the University of Granada for permitting us to use the material for the granulometric analyses. Last but not least, we would like to thank the two anonymous reviewers and editor Pierluigi Pieruccini for their constructive comments on an earlier version of the manuscript.

References

Agustí, J., Piñero, P., Lozano-Fernández, I., Jiménez-Arenas, J.M., 2022. A new genus and species of arvicolid rodent (Mammalia) from the early Pleistocene of Spain. Comptes Rendus Palevol 21, 847–858. https://doi.org/10.5852/cr-palevol2022v21a39.

Alba, D.M., Carlos-Calero, J.A., Mancheño, M.A., Montoya, P., Morales, J., Rook, L., 2011. Fossil remains of *Macaca sylvanus florentina* (cocchi, 1872) (primates, cercopithecidae) from the early Pleistocene of Quibas (Murcia, Spain). J. Hum. Evol. 61, 703–718. https://doi.org/10.1016/j.jhevol.2011.09.003.

Auler, A.S., Smart, P.L., Wang, X., Piló, L.B., Edwards, R.L., Cheng, H., 2009. Cyclic sedimentation in Brazilian caves: mechanisms and palaeoenvironmental significance. Geomorphology 106, 142–153. https://doi.org/10.1016/j.geomorph.2008.09.020.

Azema, J., 1977. Étude géologique des zones externes des Cordillères bétiques aux confins des provinces d'Alicante et de Murcie (Espagne). PhD Thesis. Université Pierre et Marie Curie.

Azema, J., Montenat, C., 1975. Mapa Geológico Nacional. E 1 (50.000), 27–35.

Bar-Matthews, M., 2014. History of water in the Middle East and north africa. In: Holland, H.D., Turekian, K.K. (Eds.), Treatise on Geochemistry, second ed. Elsevier, Oxford, pp. 109–128. https://doi.org/10.1016/B978-0-08-095975-7.01210-9.

Blain, H.-A., Bailon, S., 2019. Extirpation of *Ophisaurus* (anguimorpha, anguidae) in western Europe in the context of the disappearance of subtropical ecosystems at the early-middle Pleistocene transition. Palaeogeogr. Palaeoclimatol. Palaeoecol. 520, 96–113. https://doi.org/10.1016/j.palaeo.2019.01.023.

Blain, H.-A., Bailon, S., Agustí, J., Piñero-García, P., Lozano-Fernández, I., Sevilla, P., López-García, J.M., Romero, G., Mancheño, M.A., 2014. Youngest agamid lizards from western Europe (Sierra de Quibas, Spain, late early Pleistocene). Acta Palaeontol. Pol. 59, 873–878. https://doi.org/10.4202/app.2012.0141.

Blott, S.J., Pye, K., 2012. Particle size scales and classification of sediment types based on particle size distributions: review and recommended procedures. Sedimentology 59, 2071–2096. https://doi.org/10.1111/j.1365-3091.2012.01335.x.

Bosch, R.F., White, W.B., 2018. Lithofacies and transport of clastic sediments in karst conduits. In: Karst Groundwater Contamination and Public Health. Advance in Karst Science. Springer, Cham, pp. 277–281. https://doi.org/10.1007/978-3-319-51070-5_32.

Brook, G.A., Cowart, J.B., Brandt, S.A., Scott, L., 1997. Quaternary climatic change in southern and eastern Africa during the last 300 ka: the evidence from caves in Somalia and the Transvaal region of South Africa. Z. Geomorphol. - Suppl. 108.

Brook, G.A., Nickmann, R.J., 1996. Evidence of late Quaternary environments in northwestern Georgia from sediments preserved in Red Spider Cave. Phys. Geogr. 17, 465–484. https://doi.org/10.1080/02723646.1996.10642596.

Bull, P.A., 1981. Environmental reconstruction by electron microscopy. Prog. Phys. Geogr. 5, 368–397. https://doi.org/10.1177/030913338100500302.

Caddeo, G.A., Railsback, L.B., De Waele, J., Frau, F., 2015. Stable isotope data as constraints on models for the origin of coralloid and massive speleothems: the interplay of substrate, water supply, degassing, and evaporation. Sediment. Geol. 318, 130–141.

Carlos-Calero, J.C., Montoya, P., Mancheño, M.A., Morales, J., 2006. Presencia de *Vulpes praeglacialis* (Kormos, 1932) en el yacimiento pleistoceno de la Sierra de Quibas (Abanilla, Murcia). Estud. Geol. 62, 395–400. https://doi.org/10.3989/egeol.0662134.

Campaña, I., Benito-Calvo, A., Pérez-González, A., Ortega, A., de Castro, J.B., Carbonell, E., 2017. Pleistocene sedimentary facies of the gran Dolina archaeo-paleoanthropological site (Sierra de Atapuerca, burgos, Spain). Quat. Int. 433, 68–84. https://doi.org/10.1016/j.quaint.2015.04.023.

Carbonell, E., Bermúdez de Castro, J.M., Parés, J.M., Pérez-González, A., Cuenca-Bescós, G., Ollé, A., Mosquera, M., Huguet, R., Van Der Made, J., Rosas, A., Sala, R., Vallverdú, J., García, N., Granger, D.E., Martinón-Torres, M., Rodríguez, X.P., Stock, G.M., Vergès, J.M., Allué, E., Burjachs, F., Cáceres, I., Canals, A., Benito, A., Díez, C., Lozano, M., Mateos, A., Navazo, M., Rodríguez, J., Rosell, J., Arsuaga, J.L., 2008. The first hominin of Europe. Nature 452, 465–469. https://doi.org/10.1038/NATURE06815.

Chamley, H., 1989. Clay formation through weathering. Clay sedimentology 21–50. https://doi.org/10.1007/978-3-642-85916-8_2.

Chamley, H., Debrabant, P., Candillier, A.-M., Foulon, J., et Géochimie, S., 1983. Clay mineralogical and inorganic geochemical stratigraphy of blake-bahama basin since the callovian, site 534, deep sea drilling Project leg 76. Initial Rep. Deep Sea Drill. Proj. 76, 437–451. https://doi.org/10.2973/dsdp.proc.76.113.1983.

Chung, F.H., 1975. Quantitative interpretation of X-ray diffraction patterns of mixtures. III. Simultaneous determination of a set of reference intensities. J. Appl. Crystallogr. 8, 17–19. https://doi.org/10.1107/S0021889875009454.

Coussot, P., Meunier, M., 1996. Recognition, classification and mechanical description of debris flows. Earth Sci. Rev. 40, 209–227. https://doi.org/10.1016/0012-8252(95)00065-8.

Dasgupta, P., 2003. Sediment gravity flow—the conceptual problems. Earth Sci. Rev. 62, 265–281. https://doi.org/10.1016/S0012-8252(02)00160-5.

DeConto, R., Pollard, D., Scherer, R., Powell, R., Naish, T., 2007. Antarctic climate-cryosphere response to extreme orbital forcing during Marine Isotope Stage 31. In: AGU Fall Meeting Abstracts 2007. PP41F-07.

De Wet, G.A., Castañeda, I.S., DeConto, R.M., Brigham-Grette, J., 2016. A high-resolution mid-Pleistocene temperature record from Arctic Lake El'gygytgyn: a 50 kyr super

interglacial from MIS 33 to MIS 31? Earth Planet Sci. Lett. 436, 56–63. https://doi.org/10.1016/j.epsl.2015.12.021.

Del Castillo, E., Alías Linares, M.A., Laborda-López, C., Iannicelli, C., Pal, S., Agustí, J., Piñero, P., 2023. Insights on the climatic evolution at the pre-Jaramillo to Jaramillo transition in Europe using mineralogical analysis of the Quibas paleontological site (Early Pleistocene, southern Iberian Peninsula). Spanish J. Palaeontol. 38, 1–10. https://doi.org/10.7203/sjp.27562.

Dykes, A., 2007. Mass movements in cave sediments: investigation of a ~40,000-year-old guano mudflow inside the entrance of the Great Cave of Niah, Sarawak, Borneo. Landslides 4, 279–290. https://doi.org/10.1007/s10346-006-0077-5.

Farrand, W.R., 1975. Sediment analysis of a prehistoric rockshelter: the Abri Pataud. Quat. Res. 5, 1–26. https://doi.org/10.1016/0033-5894(75)90046-0.

Farrand, W.R., 2001. Sediments and stratigraphy in rockshelters and caves: a personal perspective on principles and pragmatics. Geoarchaeology: Int. J. 16, 537–557. https://doi.org/10.1002/gea.1004.

Finlayson, G., Finlayson, C., Pacheco, F.G., Vidal, J.R., Carrión, J., Espejo, J.R., 2008. Caves as archives of ecological and climatic changes in the Pleistocene – the case of Gorham's Cave, Gibraltar. Quat. Int. 181, 55–63. https://doi.org/10.1016/j.quaint.2007.01.009.

Fleitmann, D., Burns, S.J., Mudelsee, M., Neff, U., Kramers, J., Mangini, A., Matter, A., 2003. Holocene forcing of the Indian monsoon recorded in a stalagmite from southern Oman. Science 300, 1737–1739. https://doi.org/10.1126/science.1083130.

Ford, D., Williams, P.D., 2007. Karst Hydrogeology and Geomorphology. John Wiley & Sons. https://doi.org/10.1002/9781118684986.

Galán, E., 2011. Developments in Palygorskite-Sepiolite Research: A New Outlook on These Nanomaterials. Elsevier.

Gillieson, D., 1986. Cave sedimentation in the New Guinea highlands. Earth Surf. Process. Landforms 11, 533–543.

Goldberg, P., 2000. Micromorphology and site formation at Die Kelders cave I, South Africa. J. Hum. Evol. 38, 43–90. https://doi.org/10.1006/jhev.1999.0350.

Goldberg, P., Sherwood, S.C., 2006. Deciphering human prehistory through the geoarcheological study of cave sediments. Evol. Anthropol. Issues News Rev. 15, 20–36. https://doi.org/10.1002/evan.20094.

Gornitz, V., 2009. Mineral indicators of past climates. In: Gornitz, V. (Ed.), Encyclopedia of Paleoclimatology and Ancient Environments. Encyclopedia of Earth Sciences Series. Springer, Netherlands, pp. 573–583. https://doi.org/10.1007/978-1-4020-4411-3_143.

Gurel, A., 2008. Sedimentological and mineralogical investigation of the Late Miocene successions of Aktoprak Basin (central Turkey): implications for sediment source and paleoclimates. Clay Clay Miner. 56, 660–676. https://doi.org/10.1346/CCMN.2008.0560607.

Head, M.J., Gibbard, P.L., 2005. Early-Middle Pleistocene transitions: an overview and recommendation for the defining boundary. Geol. Soc., London, Special Publ. 247, 1–18. https://doi.org/10.1144/GSL.SP.2005.247.01.01.

Hill, C.A., Polyak, V.J., Nash, D.J., Asmerom, Y., Provencio, P.P., 2017. The West water formation (hualapai plateau, Arizona, USA) as a calcrete-paleosol sequence, and its implications for the paleogene-neogene evolution of the southwestern Colorado plateau. Palaeogeogr. Palaeoclimatol. Palaeoecol. 479, 146–163. https://doi.org/10.1016/j.palaeo.2017.05.003.

Hong, H., 2010. A review on paleoclimate interpretation of clay minerals. Geol. Sci. Technol. Inf. 29, 1–8 (in Chinese).

Hong, H., Yu, N., Xiao, P., Zhu, Y., Zhang, K., Xiang, S., 2007. Authigenic palygorskite in Miocene sediments in Linxia basin, Gansu, northwestern China. Clay Miner. 42, 45–58. https://doi.org/10.1180/claymin.2007.042.1.04.

Huang, S., Hong, H., Liao, W., Wang, C., Cheng, L., Hao, X., Li, D., Bae, C.J., Wang, W., 2020. Late Pleistocene paleoenvironment of southern China: clay mineralogical and geochemical analyses from luna cave, guangxi, China. Quat. Int. 563, 78–86. https://doi.org/10.1016/j.quaint.2020.02.003.

Hunt, C., Davison, J., Inglis, R., Farr, L., Reynolds, T., Simpson, D., 2010. Site formation processes in caves: the holocene sediments of the haua fteah, cyrenaica. Libya. J. Archaeol. Sci. 37 (7), 1600–1611. https://doi.org/10.1016/j.jas.2010.01.021.

Iacovello, F., Martini, I., 2012. Provenance and geological significance of red mud and other clastic sediments of the Mugnano Cave (Montagnola Senese, Italy). Int. J. Speleol. 41 (2), 317–328. https://doi.org/10.5038/1827-806X.41.2.17.

Inglés, M., Anadón, P., 1991. Relationship of clay minerals to depositional environment in the non-marine eocene pontils group, SE ebro basin (Spain). J. Sediment. Res. 61, 926–939. https://doi.org/10.1306/D426780C-2B26-11D7-8648000102C1865D.

Joannin, S., Bassinot, F., Nebout, N.C., Peyron, O., Beaudouin, C., 2011. Vegetation response to obliquity and precession forcing during the Mid-Pleistocene Transition in Western Mediterranean region (ODP site 976). Quat. Sci. Rev. 30, 280–297. https://doi.org/10.1016/j.quascirev.2010.11.009.

Jones, B., Ng, K.-C., 1988. The structure and diagenesis of rhizoliths from cayman brac, British west indies. J. Sediment. Res. 58, 457–467. https://doi.org/10.1016/0037-0738(95)00105-0.

Kadir, S., Eren, M., 2008. The occurrence and genesis of clay minerals associated with Quaternary caliches in the Mersin area, southern Turkey. Clay Clay Miner. 56, 244–258. https://doi.org/10.1346/CCMN.2008.0560208.

Kadir, S., Eren, M., Atabey, E., 2010. Dolocretes and associated palygorskite occurrences in siliciclastic red mudstones of the Sariyer formation (Middle Miocene), southeastern side of the Çanakkale strait, Turkey. Clay Clay Miner. 58, 205–219. https://doi.org/10.1346/CCMN.2010.0580206.

Karkanas, P., Schepartz, L.A., Miller-Antonio, S., Wang, W., Huang, W., 2008. Late Middle Pleistocene climate in southwestern China: inferences from the stratigraphic record of panxian dadong cave, guizhou. Quat. Sci. Rev. 27, 1555–1570. https://doi.org/10.1016/j.quascirev.2008.05.005.

Kennett, J.P., Warkne, D.A., 1992. Late Eocene-Early Oligocene evolution of climate and marine circulation: deep-sea clay mineral evidence. Am. Geophys. Union 97–118. https://doi.org/10.1029/ar056p0097.

Kłapyta, P., Zasadni, J., Pociask-Karteczka, J., Gajda, A., Franczak, P., 2016. Late Glacial and Holocene paleoenvironmental records in the Tatra Mountains, East-Central Europe, based on lake, peat bog and colluvial sedimentary data: a summary review. Quat. Int. 415, 126–144. https://doi.org/10.1016/j.quaint.2015.10.049.

Knidiri, A., Daoudi, L., El Ouahabi, M., Rhouta, B., Rocha, F., Fagel, N., 2014. Palaeogeographic controls on palygorskite occurrence in maastrichtian-palaeogene sediments of the western high atlas and meseta basins (Morocco). Clay Miner. 49, 595–608. https://doi.org/10.1180/claymin.2014.049.4.08.

Kourampas, N., Simpson, I.A., Perera, N., Deraniyagala, S.U., Wijeyapala, W., 2009. Rockshelter sedimentation in a dynamic tropical landscape: late Pleistocene–Early Holocene archaeological deposits in Kitulgala Beli-lena, southwestern Sri Lanka. Geoarchaeology: Int. J. 24, 677–714. https://doi.org/10.1002/gea.20287.

Lawson, T.J., 1995. An analysis of sediments in caves in the Assynt area, NW Scotland. Cave Karst Sci. 22, 3–30.

Lee, B., 2016. *Hylopetes sipora*. The IUCN Red List of Threatened Species 2016: e. T10606A22243951. https://doi.org/10.2305/IUCN.UK.2016-2.RLTS.T10606A22243951.en.

Leroy, S.A., Arpe, K., Mikolajewicz, U., 2011. Vegetation context and climatic limits of the Early Pleistocene hominin dispersal in Europe. Quat. Sci. Rev. 30, 1448–1463. https://doi.org/10.1016/j.quascirev.2010.01.017.

Lisiecki, L.E., Raymo, M.E., 2005. A Pliocene-Pleistocene stack of 57 globally distributed benthic δ18O records. Paleoceanography 20, 1–17. https://doi.org/10.1029/2004PA001071.

Lozano-Fernández, I., Blain, H.-A., Agustí, J., Piñero, P., Barsky, D., Ivorra, J., Bourguignon, L., 2019. New clues about the late Early Pleistocene peopling of western Europe: small vertebrates from the Bois-de-Riquet archeo-paleontological site (Lézignan-La-Cèbe, southern France). Quat. Sci. Rev. 219, 187–203. https://doi.org/10.1016/j.quascirev.2019.07.015.

Made, J. van der, Carlos-Calero, J.A., Mancheño, M.A., 2008. New material of the goat *Capra alba* from the Lower Pleistocene of Quibas and Huéscar (Spain). Notes on sexual dimorphism, stratigraphic distribution and systematic. Boll. Soc. Paleontol. Ital. 47, 13–23.

Margari, V., Hodell, D.A., Parfitt, S.A., Ashton, N.M., Grimalt, J.O., Kim, H., Yun, K.-S., Gibbard, P.L., Stringer, C.B., Timmermann, A., 2023. Extreme glacial cooling likely led to hominin depopulation of Europe in the Early Pleistocene. Science 38, 693–699. https://doi.org/10.1126/science.adf4445.

Montoya, P., Alberdi, M., Blázquez, A., Barbadillo, L., Fumanal, M.P., Made, J. van der, Marín, J., Molina, A., Morales, J., Murelaga, X., Peñalver, E., Robles, F., Ruiz Bustos, A., Sánchez, A., Sanchiz, B., Soria, D., Szyndlar, Z., 1999. La fauna del Pleistoceno inferior de la Sierra de Quibas (Abanilla, Murcia). Estud. Geol. 55, 127–162. https://doi.org/10.3989/egeol.

Montoya, P., Alberdi, M.T., Barbadillo, L.J., Made, J. van der, Morales, J., Murelaga, X., Peñalver, E., Robles, F., Bustos, A.R., Sánchez, A., Sanchiz, B., Soria, S., Szyndlar, Z., 2001. Une faune très diversifiée du Pléistocène inférieur de la Sierra de Quibas (province de Murcia, Espagne). Comptes Rendus de l'Académie des Sci., Ser. IIa 332, 387–393.10.1016/S1251-8050(01)01544-0.

Moore, D.M., Reynolds Jr., R.C., 1989. X-Ray *Diffraction And the Identification And Analysis Of Clay Minerals*. Oxford University Press (OUP), p. 322. https://doi.org/10.1346/CCMN.1990.0380416.

Oliveira, D., Goñi, M.F.S., Naughton, F., Polanco-Martínez, J., Jiménez-Espejo, F.J., Grimalt, J.O., Martrat, B., Voelker, A.H., Trigo, R., Hodell, D., 2017. Unexpected weak seasonal climate in the western Mediterranean region during MIS 31, a high-insolation forced interglacial. Quat. Sci. Rev. 161, 1–17. https://doi.org/10.1016/j.quascirev.2017.02.013.

Osborne, R.L., 1984. Lateral facies changes, unconformities and stratigraphic reversals: their significance for cave sediment stratigraphy. Cave Sci. 11, 175–184.

Palomo, L., Gisbert, J., 2002. *Atlas de los mamíferos terrestres de España*. Direccion General de Conservacion de la Naturaleza. SECEM–SECEMU, Madrid.

Parés, J.M., Álvarez, C., Sier, M., Moreno, D., Duval, M., Woodhead, J., Ortega, A., Campaña, I., Rosell, J., Bermúdez de Castro, J.M., 2018. Chronology of the cave interior sediments at Gran Dolina archaeological site, Atapuerca (Spain). Quat. Sci. Rev. 186, 1–16. https://doi.org/10.1016/j.quascirev.2018.02.004.

Pawelec, H., 2006. Origin and palaeoclimatic significance of the Pleistocene slope covers in the Cracow Upland, southern Poland. Geomorphology 74, 50–69. https://doi.org/10.1016/j.geomorph.2005.07.010.

Pérez-García, A., Murelaga, X., Mancheño, M.Á., Rodríguez, A.A., Romero, G., 2015. The tortoises from the lower Pleistocene palaeontological site of Quibas (región de Murcia, Spain). Comptes Rendus Palevol 14, 589–603. https://doi.org/10.1016/j.crpv.2015.01.002.

Pickering, R., Hancox, P.J., Lee-Thorp, J.A., Grün, R., Mortimer, G.E., McCulloch, M., Berger, L.R., 2007. Stratigraphy, U-Th chronology, and paleoenvironments at Gladysvale Cave: insights into the climatic control of South African hominin-bearing cave deposits. J. Hum. Evol. 53, 602–619. https://doi.org/10.1016/j.jhevol.2007.02.005.

Piñero, P., Alberdi, M.T., 2015. Estudio de los caballos del yacimiento de Quibas, Pleistoceno Inferior final (Abanilla, Murcia, España). Estud. Geol. 71, e034. https://doi.org/10.3989/egeol.

Piñero, P., Agustí, J., Blain, H.-A., Laplana, C., 2016. Paleoenvironmental reconstruction of the Early Pleistocene site of Quibas (SE Spain) using a rodent assemblage. Comptes Rendus Palevol 15, 659–668. https://doi.org/10.1016/j.crpv.2015.06.009.

Piñero, P., Agustí, J., Laborda, C., Duval, M., Zhao, J.-x., Blain, H.-A., Furió, M., Laplana, C., Rosas, A., Sevilla, P., 2022. Quibas-Sima: a unique 1 ma-old vertebrate

succession in southern Iberian Peninsula. Quat. Sci. Rev. 283, 107469 https://doi.org/10.1016/J.QUASCIREV.2022.107469.

Piñero, P., Agustí, J., Oms, O., Blain, H.-A., Furió, M., Laplana, C., Sevilla, P., Rosas, A., Vallverdú, J., 2020. First continuous pre-Jaramillo to Jaramillo terrestrial vertebrate succession from Europe. Sci. Rep. 10, 1901. https://doi.org/10.1038/s41598-020-58404-w.

Piñero, P., Agustí, J., Blain, H.-A., Furió, M., Laplana, C., 2015. Biochronological data for the Early Pleistocene site of Quibas (SE Spain) inferred from rodent assemblage. Geol. Acta 13, 229–241. https://doi.org/10.1344/GeologicaActa2015.13.3.5.

Pleguezuelos, J.M., Santos, X., 2004. Vipera latasti. In: Pleguezuelos, J.M., Márquez, M., Lizanam, M. (Eds.), Atlas y libro rojo de los Anfibios y Reptiles de España. Dirección General de Conservación de la Naturaleza, Asociación Herpetológica Española, pp. 298–300.

Pleguezuelos, J.M., 1997. *Malpolon monspessulanus* (hermann, 1804). In: Salvador, A. (Ed.), Fauna Ibérica, 10. Museo Nacional de Ciencias Naturales, pp. 408–427.

Pons, A., Campy, M., Guiot, J., 1989. The last climatic cycle in France: the diversity of records. Quat. Int. 3, 49–55. https://doi.org/10.1016/1040-6182(89)90073-6.

Rodríguez Estrella, T., Mancheño, M.Á., Romero, G., Hernández, J., 2004. Características geológicas de la Sierra de Quibas (Abanilla, Murcia). Su relación con un yacimiento paleontológico pleistoceno. Geogaceta 35, 115–118.

Rosas, A., Galli, E., Fidalgo, D., García Tabernero, A., Huguet Pamiès, R., Martínez, D., Piñero, P., Agustí, J., Rico Barrio, A., Vallverdú Poch, J., 2022. The Quibas site (Murcia, Spain): new herbivores form the Early-Middle Pleistocene transition. Riv. Ital. Paleontol. Stratigr. 128, 745–772.

Rosas, A., Soler-Fajardo, A., García-Tabernero, A., Huguet Pàmies, R., Vallverdú, J., Fidalgo, D., Galli, E., Piñero, P., Agustí, J., Valenciano, A., 2023. 2D Geometric morphometrics of the first lower molar of the genus *Meles* Brisson, 1762 including new badger evidence from the Lower Pleistocene Quibas site (Murcia, Spain). Comptes Rendus Palevol 22, 91–107. https://doi.org/10.5852/cr-palevol2023v22a7.

Sevilla, P., Agustí, J., Blain, H.-A., Laplana, C., Romero, G., Mancheño, M.A., 2014. Los murciélagos del Pleistoceno inferior de Quibas (Abanilla, Murcia, España). In: Royo-Torres, R., Verdú, F.J., Acalá, L. (Eds.), XXX Jornadas de la Sociedad española de Paleontología, vol. 24. ¡Fundamental!, pp. 229–231.

Shahack-Gross, R., Berna, F., Karkanas, P., Weiner, S., 2004. Bat guano and preservation of archaeological remains in cave sites. J. Archaeol. Sci. 31, 1259–1272. https://doi.org/10.1016/j.jas.2004.02.004.

Singer, A., 1979. Palygorskite in sediments: detrital, diagenetic or neoformed—a critical review. Geol. Rundsch. 68, 996–1008. https://doi.org/10.1007/BF01820193.

Singer, A., 1980. The paleoclimatic interpretation of clay minerals in soils and weathering profiles. Earth Sci. Rev. 15, 303–326. https://doi.org/10.1016/0012-8252(80)90113-0.

Singer, A., 1984. The paleoclimatic interpretation of clay minerals in sediments—a review. Earth Sci. Rev. 21, 251–293. https://doi.org/10.1016/0012-8252(84)90055-2.

Singer, A., 1989. Palygorskite and sepiolite group minerals. Minerals in Soil Environ. 1, 829–872.10.2136/sssabookser1.2ed.

Singer, B.S., 2014. A Quaternary geomagnetic instability time scale. Quat. Geochronol. 21, 29–52. https://doi.org/10.1016/j.quageo.2013.10.003.

Singer, A., Norrish, K., 1974. Pedogenic palygorskite occurrences in Australia. Am. Mineral. 59, 508–517. https://doi.org/10.1016/S0070-4571(08)70037-2.

Springer, G.S., 2012. Clastic sediments in caves. In: Culver, D.C., White, W.B. (Eds.), Encyclopedia of Caves. Elsevier, Amsterdam, pp. 134–140. https://doi.org/10.1007/978-1-4020-4409-0_151.

Srodon, J., 1984. X-ray powder diffraction identification of illitic materials. Clay Clay Miner. 32, 337. https://doi.org/10.1346/CCMN.1984.0320501.

Straus, L.G., 2001. Africa and Iberia in the Pleistocene. Quat. Int. 75, 91–102. https://doi.org/10.1016/S1040-6182(00)00081-1.

Teitler, L., Kupp, G., Warnke, D., Burckle, L., 2007. Evidence for a long warm interglacial during Marine Isotope Stage 31: comparison of two studies at proximal and distal ODP sites in the Southern Ocean. In: Cooper, A.K., et al. (Eds.), Antarctica: A Keystone in a Changing World – Online Proceedings of the 10th ISAES X, vol. 1047. USGS Open-File Report, p. 4. https://doi.org/10.1016/j.marmicro.2009.03.002.

Thiry, M., 2000. Palaeoclimatic interpretation of clay minerals in marine deposits: an outlook from the continental origin. Earth Sci. Rev. 49, 201–221. https://doi.org/10.1016/S0012-8252(99)00054-9.

Toro-Moyano, I., Martínez-Navarro, B., Agustí, J., Souday, C., de Castro, J.M.B., Martinón-Torres, M., Fajardo, B., Duval, M., Falguères, C., Oms, O., Pares, J.M., Anadon, P., Julia, R., García-Aguilar, J.M., Moigne, A.-M., Espigares, M.P., Ros-Montoya, S., Palmqvist, P., 2013. The oldest human fossil in Europe, from Orce (Spain). J. Hum. Evol. 65, 1–9. https://doi.org/10.1016/j.jhevol.2013.01.012.

Vaks, A., Bar-Matthews, M., Ayalon, A., Matthews, A., Halicz, L., Frumkin, A., 2007. Desert speleothems reveal climatic window for African exodus of early modern humans. Geology 35, 831–834. https://doi.org/10.1130/G23794A.1.

Vaks, A., Bar-Matthews, M., Ayalon, A., Schilman, B., Gilmour, M., Hawkesworth, C.J., Frumkin, A., Kaufman, A., Matthews, A., 2003. Paleoclimate reconstruction based on the timing of speleothem growth and oxygen and carbon isotope composition in a cave located in the rain shadow in Israel. Quat. Res. 59, 182–193. https://doi.org/10.1016/S0033-5894(03)00013-9.

Walker, M.J., López-Martínez, M., Carrión-García, J.S., Rodríguez-Estrella, T., Del-Toro, M.S.N., Schwenninger, J.L., et al., 2013. Cueva Negra del Estrecho del Río Quípar (Murcia, Spain): a late Early Pleistocene hominin site with an "Acheulo-Levalloiso-Mousteroid" Palaeolithic assemblage. Quat. Int. 294, 135–159. https://doi.org/10.1016/j.quaint.2012.04.038.

Wagner, T., Fritz, H., Stuwe, K., Nestroy, O., Rodnight, H., Hellstrom, J., Benischke, R., 2011. Correlations of cave levels, stream terraces and planation surfaces along the River Mur - timing of landscape evolution along the eastern margin of the Alps. Geomorphology 134, 62–78. https://doi.org/10.1016/j.geomorph.2011.04.024.

White, W.B., 2007a. Cave sediments and paleoclimate. J. Cave Karst Stud. 69, 76–93.

Weaver, C.E., Beck, K.C., 1977. Miocene of the SE United States: a model for chemical sedimentation in a peri-marine environment. Sediment. Geol. 17, IX–234. https://doi.org/10.1016/0037-0738(78)90003-9.

Weiner, S., Goldberg, P., Bar-Yosef, O., 2002. Three-dimensional distribution of minerals in the sediments of Hayonim Cave, Israel: diagenetic processes and archaeological implications. J. Archaeol. Sci. 29, 1289–1308. https://doi.org/10.1006/jasc.2001.0790.

White, W.B., 2007b. A brief history of karst hydrogeology: contributions of the NSS. J. Cave Karst Stud. 69, 13–26.

Woodward, J.C., Goldberg, P., 2001. The sedimentary records in Mediterranean rockshelters and caves: archives of environmental change. Geoarchaeology: Int. J. 16, 327–354. https://doi.org/10.1002/gea.1007.

Wright, V.P., Tucker, M.E., 1991. Calcretes: an introduction. In: Wright, V.P., Tucker, M. E. (Eds.), Calcretes: International Association of Sedimentologists, Reprint Series, vol. 2. Blackwell, Oxford, pp. 1–22. https://doi.org/10.1002/9781444304497.ch.

Ye, C., Yang, Y., Fang, X., Hong, H., Zhang, W., Yang, R., Song, B., Zhang, Z., 2018. Mineralogical and geochemical discrimination of the occurrence and genesis of palygorskite in Eocene sediments on the northeastern Tibetan Plateau. G-cubed 19, 567–581. https://doi.org/10.1002/2017GC007060.

Yravedra, J., Solano, J.A., Courtenay, L.A., Saarinen, J., Linares-Matás, G., Luzón, C., Serrano-Ramos, A., Herranz-Rodrigo, D., Cámara, J.M., Ruiz, A., Titton, S., Rodríguez-Alba, J.J., Mielgo, C., Blain, H.-A., Agustí, J., Sánchez-Bandera, C., Montilla, E., Toro-Moyano, I., Fortelius, M., Oms, O., Barsky, D., Jiménez-Arenas, J. M., 2021. Use of meat resources in the early Pleistocene assemblages from fuente nueva 3 (orce, Granada, Spain). Archaeol. Anthropol. Sci. 13, 213. https://doi.org/10.1007/S12520-021-01461-7.